

**Attachment 5**

**Westinghouse Electric Company LLC WCAP-17345-NP, Rev. 0,  
"H\*: Resolution of NRC Technical Issue Regarding Tubesheet Bore Eccentricity  
(Model 44F 3-Loop and Model 51F)" (Non-Proprietary) - November 2010**

**Virginia Electric and Power Company  
(Dominion)  
Surry Power Station Unit 2**

Westinghouse Non-Proprietary Class 3

WCAP-17345-NP  
Revision 0

November 2010

**H\*: Resolution of NRC  
Technical Issue  
Regarding Tubesheet  
Bore Eccentricity  
(Model 44F 3-Loop and  
Model 51F)**



**Westinghouse**

**WCAP-17345-NP**  
**Revision 0**

**H\*: Resolution of NRC Technical Issue Regarding Tubesheet  
Bore Eccentricity (Model 44F 3-Loop and Model 51F)**

**W.J. Bedont\***  
SG Management Programs

**C.D. Cassino\***  
SG Management Programs

**A.O. Roslund\***  
SG Management Programs

**G.W. Whiteman \***  
SG Management Programs

**November 2010**

Reviewer: **H.O. Lagally\***  
SG Management Programs

Approved: **D.A. Testa\*, Manager**  
SG Management Programs

*\*Electronically approved records are authenticated in the electronic document management system.*

---

Westinghouse Electric Company LLC  
1000 Westinghouse Drive  
Cranberry Township, PA 16066

© 2010 Westinghouse Electric Company LLC  
All Rights Reserved

---

---

**TABLE OF CONTENTS**

LIST OF TABLES .....	iv
LIST OF FIGURES .....	vi
1 INTRODUCTION .....	1-1
1.1 ORIGINAL NRC RAI RESOLUTION ACTION PLAN DISCUSSION .....	1-1
1.2 REVISED NRC RAI RESOLUTION ACTION PLAN DISCUSSION .....	1-2
1.2.1 Road Map to Final Response to 14 NRC RAI Except RAI # 5 and RAI# 12 .....	1-2
1.2.2 Need for Alternate Leakage Factor Approach .....	1-2
1.2.3 C <sup>2</sup> Model Contact Pressures Results .....	1-3
1.2.4 Process for Determining the Limiting H* Value .....	1-3
1.3 REFERENCES .....	1-6
2 SQUARE CELL (C <sup>2</sup> ) MODEL ANALYSIS .....	2-1
2.1 PURPOSE OF THE C <sup>2</sup> ANALYSIS .....	2-1
2.2 DEFINITION OF THE C <sup>2</sup> MODEL .....	2-3
2.3 APPLICATION OF BOUNDARY CONDITIONS .....	2-7
2.3.1 Deformation of Tubesheet Cell Edges .....	2-7
2.3.2 Applying the Internal and Crevice Pressures in the Square Cell Model .....	2-8
2.4 DISCUSSION OF MATERIAL PROPERTIES .....	2-9
2.5 CONTACT MODELING DISCUSSION .....	2-10
2.6 DISCUSSION OF BENCHMARK MODEL FOR C <sup>2</sup> MODEL COMPARISON .....	2-11
2.6.1 Thick Shell Model to Describe Finite Element Model .....	2-11
2.7 REFERENCES .....	2-18
3 STRUCTURAL CALCULATIONS FOR H* .....	3-1
3.1 OVERVIEW OF THE STRUCTURAL ANALYSIS FOR H* .....	3-1
3.2 STRUCTURAL ANALYSES (3-D FEA MODEL) .....	3-2
3.2.1 Method Discussion .....	3-2
3.2.2 Discussion of Significant Assumptions .....	3-3
3.2.3 Input .....	3-4
3.2.4 Geometry .....	3-4
3.2.5 Mesh Discussion .....	3-5
3.2.6 Tubesheet Equivalent Properties .....	3-5
3.2.7 Boundary Conditions .....	3-5
3.2.8 Tubesheet Complex 3-D FEA Analysis Results .....	3-6
3.3 CALCULATION OF MEAN H* FROM C <sup>2</sup> MODEL .....	3-16
3.3.1 Method Discussion .....	3-16
3.3.2 Development of Displacements for Square Cell .....	3-16
3.3.3 Discussion of Significant Assumptions .....	3-17
3.3.4 Input .....	3-18
3.3.5 Geometry .....	3-18
3.3.6 Mesh .....	3-18
3.3.7 Boundary Conditions .....	3-21
3.3.8 C <sup>2</sup> FEA Results .....	3-22
3.3.9 Model 44F (Turkey Point 3 & 4) FEA Results .....	3-22
3.3.10 Model 51F (Surry 1 & 2) FEA Results .....	3-22

---

3.3.11	Model 44F Contact Pressure Profiles .....	3-22
3.3.12	Model 51F Contact Pressure Profiles .....	3-22
3.3.13	Mean H* Calculations .....	3-41
3:4	CALCULATION OF PROBABILISTIC H* USING THE C2 MODEL .....	3-42
3.4.1	Assumptions .....	3-42
3.4.2	Methods Discussion.....	3-43
3.4.3	Input.....	3-47
	The necessary inputs for the probabilistic analysis using the C <sup>2</sup> model are: .....	3-47
3.4.4	Model 44F Results.....	3-48
3.4.5	Model 51F Results.....	3-48
3.5	POISSON CONTRACTION EFFECT ON H* .....	3-58
3.5.1	Methods Discussion.....	3-58
3.5.2	Discussion of Significant Assumptions .....	3-58
3.5.3	Input.....	3-58
3.5.4	Calculation of Radial Dilation.....	3-59
3.5.5	Calculation of Contact Pressure Reduction from Poisson Effect .....	3-59
3.5.6	Calculation of Increase in H* Values.....	3-61
3.6	REFERENCES .....	3-71
4	C <sup>2</sup> MODEL LEAKAGE INTEGRITY DISCUSSION .....	4-1
4.1	REFERENCES .....	4-3
5	REPORT SUMMARY AND CONCLUSIONS.....	5-1
5.1	REFERENCES .....	5-5

---

**LIST OF TABLES**

Table 2-1 Free Radial Expansion of a Tube .....	2-15
Table 2-2 Difference Between Radial Dilation of the Tube Bore and Tube .....	2-15
Table 2-3 Rigid Collar Model Input Parameters (Tube) .....	2-16
Table 2-4 Rigid Collar Model Input Parameters (Tubesheet) .....	2-16
Table 2-5 Rigid Collar Model Contact Pressure Results .....	2-17
Table 2-6 Calculated Tubesheet Inner Diameter Dilatation .....	2-17
Table 2-7 Comparison of C <sup>2</sup> and Thick Shell Results .....	2-17
Table 3-1 Input Boundary Conditions for Model 51F (Surry) .....	3-7
Table 3-2 Input Boundary Conditions for Model 44F (Turkey Point) .....	3-7
Table 3-3 Modulus of Elasticity for Materials .....	3-8
Table 3-4 Coefficient of Thermal Expansion for Materials .....	3-8
Table 3-5 Interpolated Ratios of Equivalent Material Properties for Analysis of Perforated Plate .....	3-8
Table 3-6 Equivalent Properties for Tubesheet for Model 51F SG (Surry) .....	3-9
Table 3-7 Equivalent Properties for Tubesheet for Model 44F SG (Turkey Point) .....	3-9
Table 3-8 Model 44F Turkey Point 3 & 4 Inputs and Results, 2.655 in Radius .....	3-23
Table 3-9 Model 44F Turkey Point 3 & 4 Inputs and Results, 7.291 in Radius .....	3-24
Table 3-10 Model 44F Turkey Point 3 & 4 Inputs and Results, 18.171 in Radius .....	3-25
Table 3-11 Model 44F Turkey Point 3 & 4 Inputs and Results, 28.210 in Radius .....	3-26
Table 3-12 Model 44F Turkey Point 3 & 4 Inputs and Results, 34.598 in Radius .....	3-27
Table 3-13 Model 44F Turkey Point 3 & 4 Inputs and Results, 48.288 in Radius .....	3-28
Table 3-14 Model 51F Surry 1 & 2 Inputs and Results, 4.016 in Radius .....	3-29
Table 3-15 Model 51F Surry 1 & 2 Inputs and Results, 11.722 in Radius .....	3-30
Table 3-16 Model 51F Surry 1 & 2 Inputs and Results, 20.498 in Radius .....	3-31
Table 3-17 Model 51F Surry 1 & 2 Inputs and Results, 30.193 in Radius .....	3-32
Table 3-18 Model 51F Surry 1 & 2 Inputs and Results, 48.613 in Radius .....	3-33
Table 3-19 Model 51F Surry 1 & 2 Inputs and Results, 58.308 in Radius .....	3-34
Table 3-20 H* Input Summary .....	3-41
Table 3-21 Summary of H* Mean Values .....	3-41
Table 3-22 Required Probabilistic Estimate for H* .....	3-54

---

Table 3-23 Monte Carlo Data Used in Comparative Probabilistic Analysis.....	3-54
Table 3-24 Limiting Operating Condition and TS Radius for H* Square Cell Analysis .....	3-55
Table 3-25 Typical Monte Carlo Result Output.....	3-55
Table 3-26 Positive Variations about the Mean TS CTE Used for FEA .....	3-55
Table 3-27 Negative Variations about the Mean Tube CTE used for FEA .....	3-56
Table 3-28 Bounding Model 44F H* Results for Comparison Study .....	3-56
Table 3-29 Summary of Model 44F Probabilistic Estimates .....	3-56
Table 3-30: Bounding Model 51F H* Results for Comparison Study .....	3-57
Table 3-31: Summary of Model 51F Probabilistic Estimates .....	3-57
Table 3-32 Calculation of Radial Dilation Due to Poisson Effects Model 51F and 3-Loop 44F SGs ...	3-62
Table 3-33 Calculation of Elastic Constants .....	3-62
Table 3-34 Calculation of Reduction in Contact Pressure from Poisson Effects.....	3-63
Table 3-35 Baseline and Adjusted H* Calculation for Model 51F (Surry Units 1 & 2).....	3-63
Table 3-36 Baseline and Adjusted H* Calculation for Model 44F (Turkey Point Units 3 & 4).....	3-64
Table 3-37 Distance for Poisson Effect to Attenuate .....	3-64
Table 3-38 H* Calculation for Model 51F Including Poisson Attenuation (Surry Units 1&2) .....	3-65
Table 3-39 H* Calculation for Model 44F including Poisson Attenuation (Turkey Point Units 3 & 4).....	3-65
Table 3-40 Comparison of Mean H* Values .....	3-66
Table 3-41 Baseline and Adjusted H* Calculation for Model 51F (Surry Units 1 & 2).....	3-66
Table 3-42 Baseline and Adjusted H* Calculation for Model 44F (Turkey Point Units 3 & 4).....	3-67
Table 3-43. Distance for Poisson Effect to Attenuate Probabilistic H* Values.....	3-67
Table 3-44 H* Calculation for Model 51F including Poisson Attenuation (Surry Units 1 & 2).....	3-68
Table 3-45 H* Calculation for Model 44F Including Poisson Attenuation (Turkey Point Units 3 & 4).....	3-69
Table 3-46 Comparison of Probabilistic H* Values (inches) .....	3-69
Table 5-1 Results of Probabilistic Comparison Study for the Limiting Plants for Models 44F and 51F..	5-4

---

**LIST OF FIGURES**

Figure 2-1 Current Licensing Basis Tubesheet Bore Displacements .....	2-2
Figure 2-2 C <sup>2</sup> Model Tubesheet Bore Displacements .....	2-2
Figure 2-3 Typical Lower SG Complex Model .....	2-4
Figure 2-4 Square Cell Model “Core Sample” .....	2-4
Figure 2-5 Square Cell Model.....	2-4
Figure 2-6 Typical Square Cell Coordinate System.....	2-5
Figure 2-7 Typical Square Model without Symmetry Conditions .....	2-5
Figure 2-8 Typical Square Cell Mesh with Quarter Symmetry Conditions .....	2-6
Figure 2-9 Sketches of Possible C <sup>2</sup> Model Response to Applied Displacement.....	2-8
Figure 2-10 Tube and TS Collar Assembly.....	2-12
Figure 2-11 Constant Tubesheet Bore Dilation Model .....	2-12
Figure 3-1 Typical Representation of Severed Divider Plate Condition; Model 51F .....	3-10
Figure 3-2 Typical Solid Model for Intact Divider Plate; Model 44F.....	3-10
Figure 3-3 3-D FEA Mesh, View Down Z-axis .....	3-11
Figure 3-4 3-D FEA Mesh, View Down Y-Axis .....	3-11
Figure 3-5 3-D FEA Mesh, View Down X-Axis.....	3-12
Figure 3-6 3-D FEA Results of NOP Thermal Analysis .....	3-12
Figure 3-7 3-D FEA Results of Thermal-Structural Analysis, Y Deformation .....	3-13
Figure 3-8 3-D FEA Results of Thermal-Structural Analysis, X Deformation on Hot Leg Face .....	3-13
Figure 3-9 3-D FEA Results of Thermal-Structural Analysis, Z Deformation on Hot Leg .....	3-14
Figure 3-10 3-D FEA Results of SLB Thermal Analysis.....	3-14
Figure 3-11 3-D FEA Results of SLB Thermal-Structural Analysis, X Deformation on Hot Leg Face .....	3-15
Figure 3-12 3-D FEA Results of SLB Thermal-Structural Analysis, Z Deformation on Hot Leg.....	3-15
Figure 3-13 Sub-Model for Computational Analysis.....	3-16
Figure 3-14 Representative Solid Model .....	3-19
Figure 3-15 Representative Dimensions for All Models.....	3-19
Figure 3-16 Implemented Model Mesh, View Down Z-Axis .....	3-20
Figure 3-17 Boundary Conditions for All Models .....	3-21
Figure 3-18 Model 44F Contact Pressure Results, 2.655 in Radius .....	3-35

---

Figure 3-19 Model 44F Contact Pressure Results, 7.219 in Radius .....	3-35
Figure 3-20 Model 44F Contact Pressure Results, 18.171 in Radius .....	3-36
Figure 3-21 Model 44F Contact Pressure Results, 28.210 in Radius .....	3-36
Figure 3-22 Model 44F Contact Pressure Results, 34.598 in Radius .....	3-37
Figure 3-23 Model 44F Contact Pressure Results, 48.288 in Radius .....	3-37
Figure 3-24 Model 51F Contact Pressure Results, 4.016 in Radius .....	3-38
Figure 3-25 Model 51F Contact Pressure Results, 11.722 in Radius.....	3-38
Figure 3-26 Model 51F Contact Pressure Results, 20.498 in Radius .....	3-39
Figure 3-27 Model 51F Contact Pressure Results, 30.193 in Radius .....	3-39
Figure 3-28 Model 51F Contact Pressure Results, 48.613 in Radius .....	3-40
Figure 3-29 Model 51F Contact Pressure Results, 58.308 in Radius .....	3-40
Figure 3-30: Model 44F Crevice Pressure Adjustment Curve .....	3-46
Figure 3-31: Model 51F Crevice Pressure Adjustment Curve .....	3-46
Figure 3-32 Typical Result for Plotting the Combined Tube and Tubesheet .....	3-49
Figure 3-33 Typical Result for Plotting the Combined Tube and Tubesheet .....	3-49
Figure 3-34 Typical Comparative H* Curves from Selected Response Surface.....	3-50
Figure 3-35 Model 44F NOP Combined CTE <sub>T</sub> and CTE <sub>TS</sub> vs. Monte Carlo Rank Order.....	3-50
Figure 3-36 Reduced Model 44F NOP Response Data.....	3-51
Figure 3-37 Model 44F H* Summary Showing Linear Fit Results .....	3-51
Figure 3-38 Model 51F SLB Combined T CTE and TS CTE as a Function of H* .....	3-52
Figure 3-39 Reduced Model 51F SLB Response Data .....	3-52
Figure 3-40 Model 51F H* Summary Showing Linear Fit Results .....	3-53
Figure 3-41 Effect of Poisson Contraction on Contact Pressure.....	3-70

---

## 1 INTRODUCTION

The purpose of H\* is to replace the tube-end weld with the hydraulic expansion joint as the primary pressure boundary in the SG. There are two principal requirements for H\*:

1. Assure that the tube(s) do not pull out of the tubesheet under the most limiting loads during normal operating or accident conditions.
2. Assure that the primary coolant leakage through the tube-to-tubesheet crevice is no greater than the leakage assumed in the final safety analysis report (FSAR) for the most limiting accident.

In October 2009, the NRC issued its first of several approvals of H\* (Reference 1-1, typical). The approval in each case was limited to the operating period until the plant's next scheduled inspection because, as stated by the NRC, one technical issue remained to be resolved. The technical issue revolves around the relationship between tubesheet bore eccentricity and the tube-to-tubesheet contact pressure. This issue was identified in Reference 1-2, which provided 14 questions related to this issue. The purpose of this report, in conjunction with References 1-6 and 1-7, is to provide final resolution of the remaining questions in support of the permanent application of the H\* criterion. The remaining eccentricity issue impacts both the structural and leakage analysis aspects of the H\* analysis.

In this report, reference to the "current licensing basis" means the basis on which the temporary licenses were provided to the Model 44F and Model 51F plants. Principally, the technical basis for the current licensing basis is contained in WCAP-17091-P, (Reference 1-3) and WCAP-17092-P (Reference 1-4), but also includes other documents included in the respective License Amendment Requests (LARs) from the respective Model 44F and Model 51F plants.

Reference 1-3 discusses the criteria for selecting the model-specific limiting plant. Only three 3-loop plants with Model 44F SGs are in the H\* candidate population, Turkey Point Units 3 and 4 and H.B. Robinson Unit 2. Turkey Point was determined to be the limiting plant for the 3-loop Model 44F plants. Therefore, all analyses based on the Turkey Point conditions are equally applicable to H.B. Robinson as well.

Only two Model 51F plants exist, Surry Units 1 and 2, for which the design conditions are identical.

### 1.1 ORIGINAL NRC RAI RESOLUTION ACTION PLAN DISCUSSION

Westinghouse initially interpreted the thrust of the questions in Reference 1-2 as follows:

The H\* structural justification includes an analysis that determines the contact pressure between the tubes and the tubesheet. The reference model for this calculation, the "Scale Factor Model" (SF) is a previously documented model (Reference 1-5) developed to determine the contact pressure for various values of dilation and eccentricity of the tubesheet bore. The output of this model is a multiplier to be applied to the calculated value of contact pressure due to tubesheet bore dilation, which is subtracted from the contact pressure generated due to tube-to-tubesheet differential thermal and pressure expansions. Because the transient conditions for one model (D5) of the affected steam generators required application of this model for conditions outside of the applicability of the reference model, a second model, the "Square-Cell

---

Model" ( $C^2$ ) based on 2-D finite element analysis (FEA), was utilized to directly determine the contact loads between the tubes and the tubesheet for these conditions.

Both models are based on conservative analysis and assumptions; however, Westinghouse believes that the  $C^2$  model more accurately represents the physical structure. Originally, the principal purpose of the  $C^2$  model was to demonstrate that adequate contact pressure exists around the circumference of the tube under significant tubesheet bore eccentricity conditions. The two models, SF and  $C^2$ , are entirely different approaches; thus, it is not expected that the results from both models provide the same results. Westinghouse believed that, in aggregate, the NRC unresolved issue questions requested a comparison of the models and rationalization of the conservatism of the current licensing basis.

During a meeting in January 2010 with the NRC and the industry participants, Westinghouse proposed a plan to resolve all of the NRC questions through an approach believed to minimize the potential for additional questions. The NRC staff did not reject the recommended approach but stated that the 14 questions provided by Reference 1-2 must be clearly, if not directly, addressed. The target date established for a permanent H\* license was the Spring 2011 outages. It was expected at the time that the contact pressures developed using the  $C^2$  model would be of such a magnitude that the conservatism of the original licensing basis from both a structural and leakage integrity basis would be readily demonstrated.

## **1.2 REVISED NRC RAI RESOLUTION ACTION PLAN DISCUSSION**

The Westinghouse action plan to respond to the 14 RAI questions was revised as discussed below.

### **1.2.1 Road Map to Final Response to 14 NRC RAI Except RAI # 5 and RAI# 12**

It was determined by the NRC staff that the issues related to the SF model were resolved and that within the context of the SF model, eccentricity does not appear to be a significant variable affecting the tube to tubesheet contact pressure or calculated H\* distances. This conclusion is based largely on the information provided in References 1-6 and 1-7 (LTR-SGMP-10-78 P-Attachment and LTR-SGMP-10-33 P-Attachment). From this information, the NRC staff concluded in Reference 1-8 that several of the NRC questions no longer require specific answers. Reference 1-7 provides a final response for each of the 14 remaining questions except RAI Questions # 5 and #12, which address the  $C^2$  model specifically. A more detailed description of the  $C^2$  model, necessary to complete this remaining action, is provided by this report.

### **1.2.2 Need for Alternate Leakage Factor Approach**

The Darcy formulation was used in References 1-3 and 1-4 to develop the ratio of leak rates between postulated accident induced conditions (SLB) and normal operating conditions (NOP). The Feedwater Line Break (FLB) is not included in the licensing basis for the Model 44F and Model 51F steam generators. The driving heads ( $\Delta p$ ) at both of these conditions are known, as are the temperatures and pressures to define the fluid viscosity ( $\mu$ ). In References 1-3 and 1-4, because the physical length of the leak path was the same under both normal operating and accident conditions, the length of the leak path was not a factor. The only remaining factor was the loss coefficient (K). Based on the analyses using the

---

$C^2$  model, the length of the leak paths under normal operating conditions and accident conditions may differ; therefore, the SLB:NOP leak rate ratio is re-evaluated in Section 4 of this report.

The available data for hydraulically expanded tubes in tubesheet simulants (References 1-9 and 1-10), both at room temperature and at elevated temperature, were used in Reference 1-3 and 1-4 to show that no correlation between loss coefficient and contact pressure exists. However, because the data exhibit considerable scatter, confidence in this data analysis was low. Engineering judgment could suggest that loss coefficient might be related to the absolute contact pressure between the tubes and the tubesheet. Hence, a requirement was applied to the  $H^*$  leakage analysis by the regulatory authorities that it is necessary to show that the contact pressure at accident induced conditions exceeds the contact pressure at normal operating conditions ( $P_{C_{SLB}}:P_{C_{NOP}} > 1$ ). For the Model 44F and 51F steam generators, this criterion is met for application of both the Thick Shell Equation model and the  $C^2$  model. Nevertheless, alternate approaches for leakage analysis, which do not depend on loss coefficient being independent of contact pressure, were developed to show that the accident induced leakage value assumed in the FSAR is not exceeded. Two alternate leakage methods are discussed in Reference 1-10.

### 1.2.3 $C^2$ Model Contact Pressures Results

The contact pressures calculated with the  $C^2$  model do not consistently exceed the values calculated with the scale factor (SF) model. Using the  $C^2$  Model, it was determined that the magnitude of contact pressures did not increase at all tube radii at all tubesheet elevations relative to the SF analysis results during normal operating and SLB conditions. As a result of the change in contact pressures, re-calculation of the probabilistic  $H^*$  value was required for each model SG in the  $H^*$  fleet.

### 1.2.4 Process for Determining the Limiting $H^*$ Value

The final  $H^*$  depth recommended is the 95 percent probability at 50 percent confidence (95/50) estimate of  $H^*$ . Consistent with prior practice, the 95 percent probability at 95 percent confidence (95/95) estimate of  $H^*$  is also provided for information. The probabilistic  $H^*$  depth is based on the mean  $H^*$  value for the limiting tubesheet radius. As discussed in detail in References 1-3 and 1-4, the principal variables affecting the probabilistic value of  $H^*$  are the coefficients of thermal expansion of the tube and tubesheet materials. The specific values of these variables that define probabilistic analysis of  $H^*$  based on the  $C^2$  model are determined from the variability surface described in Figure 8-5 of References 1-3 and 1-4. Application of these values in the  $C^2$  model is discussed in Section 3.4 of this report. The probabilistic estimate of  $H^*$  is further adjusted by the addition of a factor to account for the Poisson contraction of the tubes due to end cap loading, and a further adjustment of the length to account for the effect of the crevice pressure distribution which is dependent on the initially predicted length of  $H^*$ . The adjustment for crevice pressure distribution is discussed in References 1-3 and 1-4 and Section 3.4 of this report. The adjustment for Poisson contraction is discussed in Section 3.5 of this report.

The limiting  $H^*$  estimate for NOP and SLB is determined for the worst case sector of the tubesheet, which is the region of the tubesheet perpendicular to the tube lane, plus or minus five degrees azimuthally (see Section 6.2.3 of References 1-3 and 1-4). The  $H^*$  estimate is determined using TS displacements from the worst case calculated using a 3-D half-symmetry finite element model of the lower SG complex described in Section 6.2.1 of References 1-3 and 1-4 and further discussed in Section 3.2 of this report. The tubesheet displacements are input to the calculation of contact pressure between the tube and the

tubesheet at nine elevations at each tubesheet radius in the limiting sector. The distribution of contact pressure as a function of elevation at a given tubesheet (TS) radius (see Section 3.3) defines the pull out resistance of a SG tube to an applied end cap load at that radius. The required  $H^*$  length is defined by the integration of the cumulative pull out resistance as a function of depth in the tubesheet. The structural model used to calculate the contact pressures between the tubesheet and the tube is a pseudo sub-model to the 3D FEA model, called the square cell model ( $C^2$  in this report). The  $C^2$  model which is a quarter symmetry model of the tube and tubesheet material in a single tube pitch subjected to applied pressure and temperature in addition to the applied displacements from the tubesheet. A separate  $C^2$  model is developed for each elevation at a single TS radius. The radial location of the worst case  $H^*$  estimate is the TS radius with the longest required engagement length to balance an end cap load of  $3\Delta P_{NOP}$  or  $1.4\Delta P_{DBA}$  (whichever condition results in a greater  $H^*$  value) assuming mean material properties. See Section 3.3 of this report for a detailed description.

The probabilistic estimate of  $H^*$  is based on a Monte Carlo simulation for determining the effect of varying the TS coefficient of thermal expansion (CTE) and the tube (T) CTE on the contact pressure based on the limiting operating condition from the mean material estimate of  $H^*$ . The final result of the simulation is the combination of TS and T CTE which defines the 95<sup>th</sup> percentile probability at a 50 percent or greater confidence estimate for increasing  $H^*$  during the limiting operating condition at the limiting TS radius. The predicted combination of CTEs from the simulation is input to the  $C^2$  model to calculate the value of  $H^*$  at the required probabilistic estimate. See Section 3.4 of this report for a detailed description.

The distribution of contact pressure for the limiting operating condition, at the limiting TS radius, at the required probabilistic estimate, is used to determine the effect of Poisson contraction on the probabilistically defined  $H^*$  value. The effect of Poisson contraction is determined by using standard thick shell equations (see Section 3.5) to calculate the reduction in contact pressure from a corresponding reduction in the outer diameter of the tube due to an applied axial end cap load on a closed thick walled pressure vessel. The net result is added to the probabilistic  $H^*$  value to increase the required engagement length of the tube portion within the tubesheet. The Poisson contraction is based on the probabilistic contact pressure profile because the probabilistic value of  $H^*$  is the basis of the requested license amendment. The crevice pressure effect is added to  $H^*$  after the probabilistic value of  $H^*$  with the Poisson effect is determined. The effect of crevice pressure on the structural analysis is described in Sections 6.4.8 and 8.1.2 of References 1-3 and 1-4 and in Section 3.4 of this report. The crevice pressure adjustment is applied after the adjustment for Poisson contraction because the Poisson contraction is an adjustment for a loading condition that is independent of the crevice pressure correction.

As a result of the issues discussed above, the action plan shifted from demonstrating the conservatism of the current licensing basis to the following:

1. Using the more accurate  $C^2$  Model to confirm that the contact pressures at accident conditions exceed those at normal operating conditions, and to demonstrate that the criterion for contact pressure ( $SLB:NOP > 1$ ) for each of the Model SGs in the  $H^*$  Fleet is met at all tubesheet bundle radii. For the Model D5 SG and for the 2 loop Model 44F SG, it was determined that the requirement  $P_{CSLB} \cdot P_{CNOP} > 1$  could not be met; therefore, two alternate means were developed to demonstrate that the leakage factors in place in the current licensing basis remain conservative for these model SGs.

- 
2. Using the more accurate  $C^2$  model, calculation of revised probabilistic  $H^*$  values for each of the models of steam generators in the  $H^*$  fleet.

Three reports are provided for the entire population of  $H^*$  candidate plants to complete the response to the Reference 1-2 (typical) questions:

- a combined report for the Model F and D5 SGs (Reference 1-11)
- a combined report for the Model 44F and 51F (3-loop plants) – this report
- a separate report for the single Model 44F 2-loop plant (to be issued)

This report addresses the  $C^2$  Model results for the Model 44F 3-loop plants and the Model 51F SGs and provides a final response to RAI Question #5 and #12. The remainder of the NRC RAI has been answered in previous submittals as discussed in Section 1.2.1 above.

---

### 1.3 REFERENCES

- 1-1. USNRC Letter, "Vogtle Electric Generating Plant, Units 1 and 2, Issuance of Amendments Regarding Technical Specifications (TS) Section 5.5.9, "Steam Generator Program," and TS 5.6.10, "Tube Inspection Report," for Interim Alternate Repair Criteria (TAC Nos. ME1339 and ME1340)," September 24, 2009.– (typical for all H\* participants)
- 1-2. USNRC Letter, "Turkey Point Nuclear Plant, Units 3 and 4 -Request for Additional Information regarding the Permanent Alternate Repair Criteria License Amendment Request (TAC Nos. ME1754 and ME1755) December 29, 2009. (typical for all H\* participants).
- 1-3. WCAP-17091-P, Revision 0, H\*: Alternate Repair Criteria for the Tubesheet Expansion Region in Steam Generators with Hydraulically Expanded Tubes (Model 44F), June 2009.
- 1-4. WCAP-17092-P, Revision 0, H\*: Alternate Repair Criteria for the Tubesheet Expansion Region in Steam Generators with Hydraulically Expanded Tubes (Model 51F), June 2009.
- 1-5. SM-94-58, Revision 1, "Doel 4 Elevated Tubesheet Sleeve – ASME Code Evaluation and Effect of Tubesheet Rotations on Contact Pressure," December 1995. (Proprietary)
- 1-6. LTR-SGMP-10-78 P-Attachment, "Effects of Tubesheet Bore Eccentricity and Dilation on Tube-to-Tubesheet Contact Pressure and their Relative Importance to H\*," September 2010.
- 1-7. LTR-SGMP-10-33 P-Attachment, "H\*: Response to NRC Questions Regarding Tubesheet Bore Eccentricity," September 2010.
- 1-8. USNRC Letter, "Vogtle Electric Generating Plant – Audit of Steam Generator H\* Amendment Reference Documents (TAC Numbers ME3003 and ME3004)," July 9, 2010.
- 1-9. STD-MCE-03-49, "Determination of Model D5 Tube-to-Tubesheet Leakage Resistance for H-star Program for CBE/DCE/DDP/TCX," November 4, 2003.
- 1-10. LTR-SGMP-10-95, Revision 1, "H\*: Alternate Leakage Calculation Methods for H\* for Situations When Contact Pressure at Normal Operating Conditions Exceeds Contact Pressure at Accident Conditions," September 3, 2010.
- 1-11. WCAP-17330-P, Revision 0, "H\*: Resolution of NRC Technical Issue Regarding Tubesheet Bore Eccentricity (Model F/Model D5)," November 2010.

## 2 SQUARE CELL ( $C^2$ ) MODEL ANALYSIS

This section provides a generic description of the  $C^2$  model. Although there are SG model-specific applications of the  $C^2$  model, the description of the  $C^2$  model is based principally on the application for the Model D5 steam generators because the model was initially developed for the Model D5 steam generators. The entire generic description of the  $C^2$  model applies equally to the Model 44F and Model 51F steam generators.

### 2.1 PURPOSE OF THE $C^2$ ANALYSIS

Figure 1-1 in the current licensing bases (References 2-1 and 2-2) defines the calculation process for  $H^*$ . The foundation for all of the structural analyses is a global model of the lower tubesheet complex (called the 3-D FEA model, see References 2-1 and 2-2) that provides the tubesheet displacements that are used to calculate tube-to-tubesheet contact pressures. In the current licensing basis for  $H^*$ , based on the thick-shell equations, tubesheet displacements generated by the bending of the tubesheet from the primary-to-secondary pressure differential in the global 3-D model are applied directly to the inner diameter of the tubesheet tube bore. This is a very conservative assumption that does not accurately represent the real physical condition.

The deflections of the tubesheet tube bore surfaces occur due to the radial thermal growth, radial pressure growth and the primary-to-secondary pressure differential acting on the tubesheet. The thermal growth of the tubesheet itself and the distortion of the tubesheet tube bore due to bending of the tubesheet under the primary-to-secondary pressure differential are transmitted to the tube bore through the tubesheet material to the ligament surrounding a given tube. The square cell model analysis ( $C^2$ ) is a conservative, more accurate, approach to modeling the process by which the tubesheet deformations are transferred to an individual tube bore. Figure 2-1 and Figure 2-2 illustrate the differences between the approach utilized in the thick shell model and that used in the square cell model in applying the displacement calculated with the 3-D FEA lower tubesheet complex model.

In Figure 2-1, the calculated local displacements are applied to the inner diameter of the tubesheet tube bore. In Figure 2-2, the calculated local displacements are applied to the outer edges of the tubesheet cell material, and the displacements at the inner diameter of the tubesheet tube bore evolve from the local structural model (the  $C^2$  model). The analysis method in Figure 2-2 is physically more realistic because it mimics the process by which the gross tubesheet displacements are transferred to the circumference of the tubesheet tube bore. The analysis method in Figure 2-1 is the simplest option for comparing the finite element model to analytical equations, i.e., the classical thick-shell equations. Also, if the geometry of the model is circular, the simplest way to apply a postulated load or displacement on the collars is to a surface which includes the inner diameter. However, because the global model does not include a distinct representation of the individual tube bore, additional assumptions must be made to determine what displacements should be applied to the boundaries of a local model (as shown in Figure 2-2) so that the tubesheet tube bore deflects in a realistic fashion.

The issue of how tubesheet tube bore deflection affects the tube-to-tubesheet contact pressure is the same regardless of the method chosen to apply displacements from the large scale model (3-D FEA) to the local sub-model. The basic problem is defined by how the large scale tubesheet deflections are transferred (or "mapped") to the local scale of a single tubesheet tube bore and tube. For the purposes of this report, the

terms large scale and global scale refer to the 3-D finite element model of the channelhead, tubesheet, divider plate and lower shell (a.k.a., "Stub Barrel") that make up a typical Westinghouse designed steam generator in the existing domestic fleet (see Figure 2-3). In the case of the prior H\* analysis (References 2-1 and 2-2), the sub-modeling is complicated by the fact that the presence of the perforations in the tubesheet are smeared throughout the perforated region in the tubesheet using the method of Slot (Reference 2-3). This means that in the global model of the lower steam generator complex the tube bores do not exist although the effect of the perforations on the structure is accounted for with respect to pressure and temperature. This is a complication for the square cell model approach because the exact displacements around a tube pitch cannot be directly taken from the 3-D finite element model of the lower SG complex.

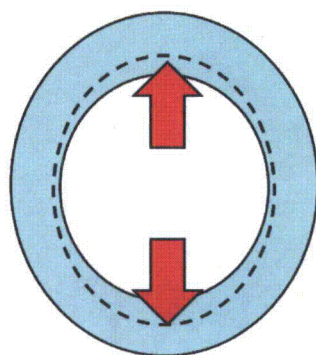


**Figure 2-1 Current Licensing Basis Tubesheet Bore Displacements**  
(local displacement applied directly to tubesheet bore)

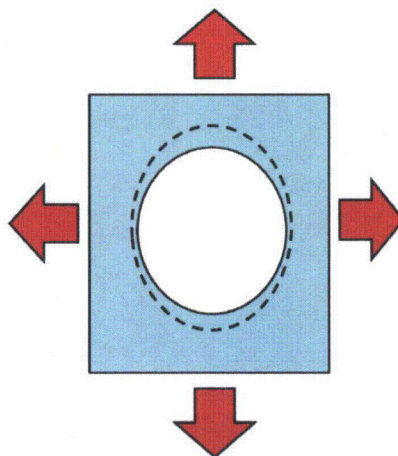


**Figure 2-2 C<sup>2</sup> Model Tubesheet Bore Displacements**  
(local displacement applied to surrounding tubesheet material)

The effect of the perforations in the non-perforated model with the effective material properties includes the expansion of the tubesheet with respect to temperature and pressure, assuming that all the tubes in the bundle are pressurized. The elastic modulus and Poisson's ratio of the perforated material are altered so that the isotropic material becomes orthotropic. This means that the stiffness of the tubesheet along different axes is different so that the expansion of the tubesheet due to the combined pressure and temperature loads is conserved without the perforations being modeled. The question remains as to how to include the effect of the individual tube bores interacting locally. That question can be accommodated using different sub-models which, in general, are not necessary to calculate the tube-to-tubesheet contact pressure. Section 6.2.3 in References 2-1 and 2-2 describe the approach to bridging the gap between a single tubesheet tube bore in an isolated model and including effects for the presence of other linked tubesheet tube bore at a local scale due to pressure at a given operating temperature. The reason they are not necessary is that along any given radial line from the center of the tubesheet it is possible to determine what the displacement is over that entire distance. This means that the displacement of a unit section can be determined but the displacement of a specific tube bore cannot be determined from the global model. In the case of H\*, the displacement of specific tubes at key radii is used in determining the average tube-to-tubesheet contact pressure.

Figure 2-3 shows a general model of the lower steam generator complex which is the source of the displacements used in the square cell analysis. The intent of the C<sup>2</sup> model is to simulate a limited thickness "core sample" of a single tube at a given radius as shown in Figure 2-4. The square cell model, shown in Figures 2-5, 2-7, and 2-8, is a local model consisting of plane stress solid elements that approximate the tube and tubesheet material defined by a one-half tube pitch around a single tubesheet tube bore through the thickness of the tubesheet (21.03 inches for the Model 51F and 21.81 inches in the Model 44F SGs). This is the definition of the unit "square cell" model of the local tubesheet tube bore. The intent of this model is to provide a physically more realistic estimate of the contact pressure between the tube and the tubesheet at various elevations through the thickness of the tubesheet during the operating condition of interest.

## 2.2 DEFINITION OF THE C<sup>2</sup> MODEL

The square cell model is based on a unit cell of tubesheet material surrounding a single tubesheet tube bore in various models of Westinghouse steam generators. Each SG model is represented by a separate square cell model. The square cell is defined by taking one-half of the nominal tube pitch around a tube as the limit of the material in the model. The initial dimensions for the square cell model are based on the room temperature unpressurized condition. For example, in a Westinghouse Model 44F SG, the tube pitch is [ ]<sup>a,c,e</sup> inches. The outer nominal tube radius is [ ]<sup>a,c,e</sup> inch. The inner nominal tube radius is [ ]<sup>a,c,e</sup> inch. The square cell is shown in Figure 2-6, with typical boundary conditions applied on the model. A quarter section of the model is used for analysis.

The square cell model is oriented in the X-Z plane of the tubesheet as defined in the lower SG complex shown in Figure 2-3. (For clarity, the square cell model is in the plane of the tubesheet but, for convenience, the square cell model is imported to ANSYS in an X-Y plane as noted in Figure 2-7.) The applied displacements, or forces, representing the net strain over the cell in the global X direction (formerly referred to in prior RAI responses as "e-bar") and the global Z direction (formerly referred to in prior RAI responses as "z-bar"). These net displacements are now referred to as  $\Delta X$  and  $\Delta Z$ .



**Figure 2-3 Typical Lower SG Complex Model**

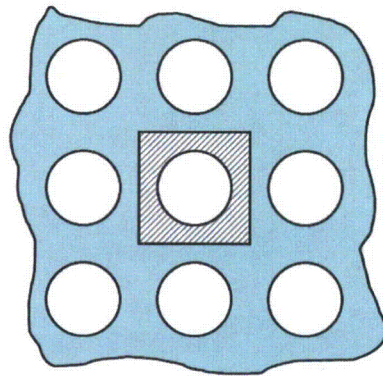


**Figure 2-4 Square Cell Model "Core Sample"**

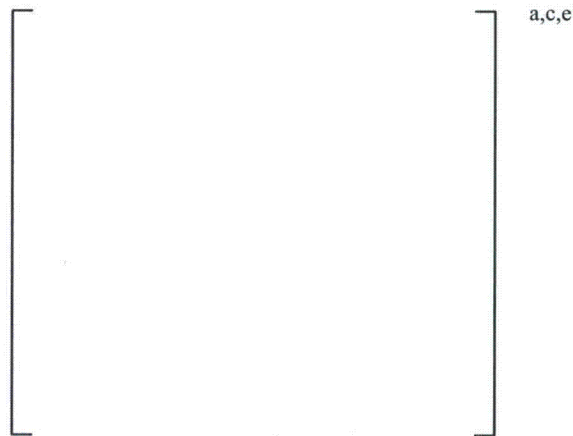


**Figure 2-5 Square Cell Model**

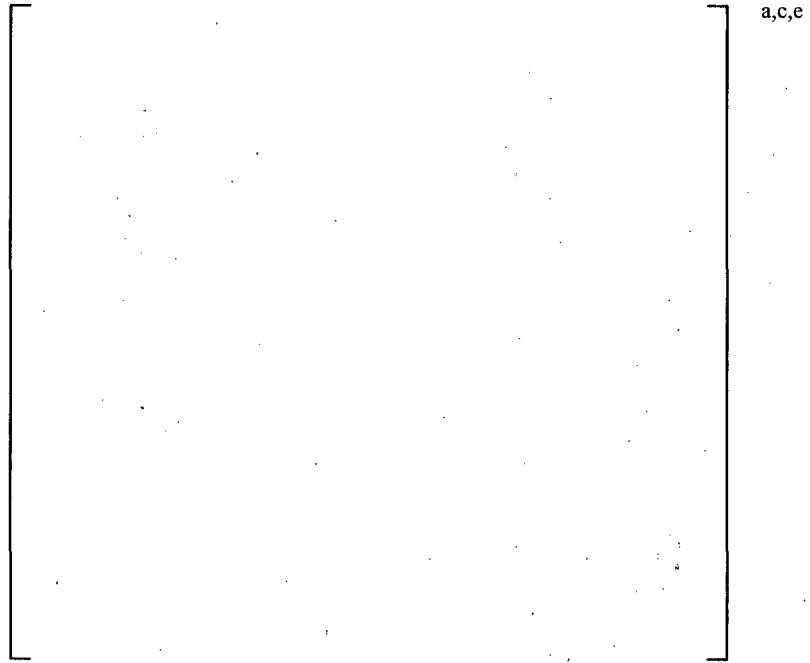


**Figure 2-6 Typical Square Cell Coordinate System**



**Figure 2-7 Typical Square Model without Symmetry Conditions**

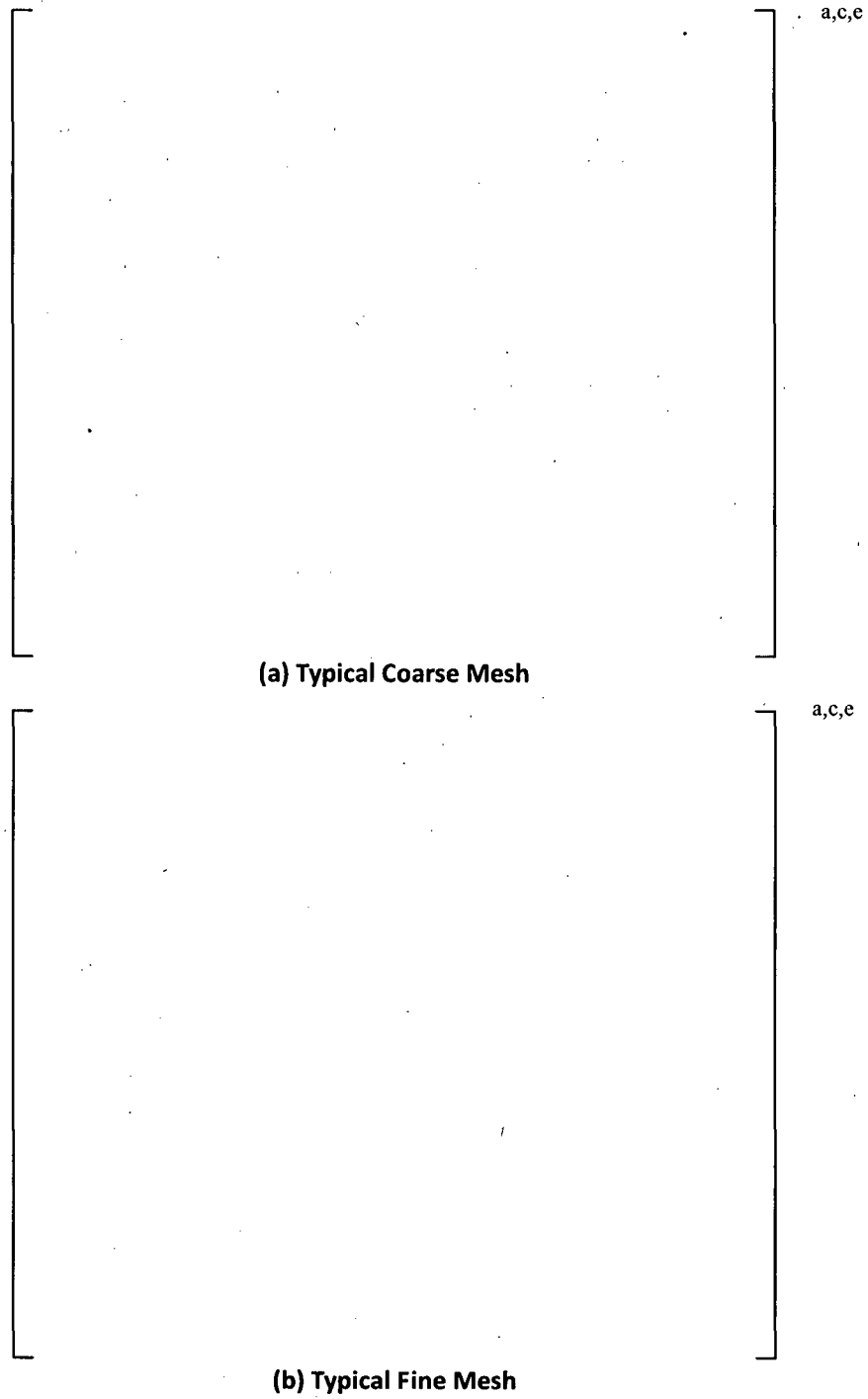


**Figure 2-8 Typical Square Cell Mesh with Quarter Symmetry Conditions**

---

## 2.3 APPLICATION OF BOUNDARY CONDITIONS

There are three categories of boundary conditions that are applied in the square cell model: thermal, pressure, and displacement. All components in the square cell model are assumed to be at a uniform temperature, depending on the operating condition, with the tube in equilibrium with the primary fluid temperature. The approaches taken in this analysis were selected because they are consistent with the current licensing basis for H\*. The discussion below summarizes the issues with each approach to applying the pressure and displacement loads to the square cell model. The impact of any installation effects from the hydraulic expansion of the tube into the tubesheet tube bore is ignored in this analysis in order to be consistent with the licensing basis used for H\*. The potential effect of any strain hardening from the expansion process can be ignored because the calculated elastic stresses in the tubes do not exceed the elastic limit of the tube material (see Section 6.2.5 of References 2-1 and 2-2).

### 2.3.1 Deformation of Tubesheet Cell Edges

Displacement based boundary conditions are used in the C<sup>2</sup> approach in a pseudo sub-model approach because the global model dictates how the sub-model should behave at the nodal level. For example, if the displacements due to the effect of temperature and pressure around the entire boundary of the sub-model are known, then those displacements can be directly applied to the sub-model. The square cell analysis is not a true sub-model analysis because the nodal displacement is not used as the applied boundary conditions. Instead, the average displacements over a tube pitch at a specified location and elevation are used. Loads which lead to additional displacements in the C<sup>2</sup> model (such as the thermal expansion of the tubesheet tube bore inner diameter) are not additive with the displacements from the initial conditions taken from the global SG model. This is because the applied displacements on the boundaries of the square cell model already account for the expansion of the tubesheet material due to pressure and temperature.

The preferred approach in the square cell analysis is to specify displacements at the boundaries of the tubesheet material as taken from the 3-D finite element model of the lower SG complex. Figure 2-9 illustrates the potential responses to the applied displacement that can occur in the square cell model.

It is important to understand that from the perspective of calculating the tube bore eccentricity based on the deflection of the major and minor axes of the tube bore all of the possibilities in Figure 2-9 (a through c) are equal. The reaction of the model to those displacements is different based on how the nodal constraints are applied. For example, in Figure 2-9a, all nodes on the boundaries are assumed to expand equally along the different axes. In Figure 2-9b, nodal constraints are used so that the end points of the tubesheet material deform the entire distance and the remainder is linearly related to the maximum displacement. In Figure 2-9c, the displacement of the two surfaces in the model develops naturally based on the applied displacement with no constraints on the nodal behavior. Figure 2-9a is the most conservative application of the displacement because it results in the lowest contact pressures. Figure 2-9b tends to maximize the eccentricity in the tubesheet tube bore. It is not likely that the outer edges of the tubesheet material will deform in this manner because the growth in the tubesheet is mainly due to thermal effects which are nearly uniform in both directions and the growth from adjacent pressurized tubesheet tube bore will also act to prevent such a deformation in the majority of the bundle. Figure 2-9c has no assumptions on the deformation of the tubesheet tube bore material and allows a non-uniform displacement to develop on either edge in response to the applied displacement. However, the majority of

the deformation in the tubesheet is due to thermal effects, which means that the tubesheet material should deform in a mostly uniform manner. Therefore, the approach shown in Figure 2-9c is not used. Figure 2-9a is the preferred approach to applying the displacement taken from the lower SG complex model because it is the most conservative for calculating  $H^*$ .

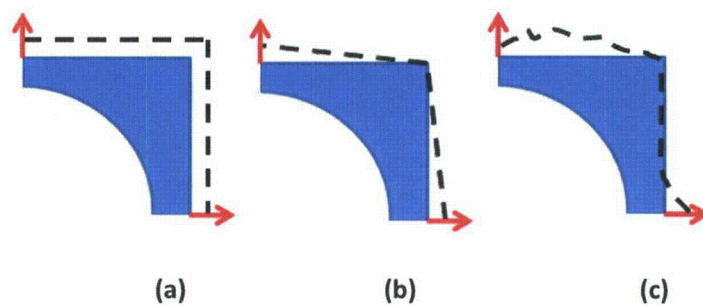


Figure 2-9 Sketches of Possible  $C^2$  Model Response to Applied Displacement

### 2.3.2 Applying the Internal and Crevice Pressures in the Square Cell Model

Two pressure loads must be accounted for in the square cell model. The first is the internal pressure acting on the inner diameter of the tube, representing the reactor coolant pressure. The second is the crevice pressure that the outer diameter of the tube and the inner diameter of the tube bore are exposed to assuming a through-wall flaw in the tube. The distribution of the crevice pressure varies according to the elevation of the tube in the tubesheet relative to the location of the flaw that allows the primary coolant into the crevice (References 2-4 and 2-5).

The internal pressure and crevice pressure can be included in the square cell model in two ways. First, the difference in the pressure acting on the outer diameter of the tube and the inner diameter of the tube can be applied as a pressure load that varies according to the elevation within the tubesheet. In this case, both the internal pressure acting on the tube and the crevice pressure are combined into the single differential pressure applied on the inner diameter of the tube. Second, the full internal pressure is applied to the inner diameter of the tube and the full crevice pressure (as a function of elevation) is applied to the outer diameter of the tube and the inner diameter of the tubesheet tube bore. The first option is the preferred approach in the square cell model because it conservatively minimizes the growth of the tube at the lower elevations of the tubesheet. This leads to a reduced contact pressure at the bottom of the tubesheet. This option is also simple to resolve with the contact options available in the structural analysis code, *ANSYS*, because a uniform pressure is pushing the outer surface of the tube into the inner surface of the tubesheet. The second crevice pressure option is difficult to resolve with the contact options in *ANSYS*.

The crevice pressure is assumed to act on 100 percent of the circumference of the outer diameter of the tube surface and inner diameter of the tubesheet tube bore. It is also simpler to account for the effect of the crevice pressure over the entire tubesheet tube bore as opposed to limited regions of the tube outer diameter. This assumption is conservative because test data (References 2-1, 2-2 and 2-5) shows that this

cannot occur. The observed leakage during the tests was more aptly characterized as “weepage,” i.e., dropwise leakage. Also, recent work reported in the literature (Reference 2-6) based on fluid structure interaction shows that fluid blanketing of the entire crevice cannot occur. Both point to evidence that supports the assumption in the analysis of record for  $H^*$  of a “tortuous path” that the liquid must take as it diffuses through the porous medium of the tube-to-tubesheet crevice. However, the nature of the test specimens, used in References 2-1, 2-2 and 2-4, make it impossible to ascertain what portion of the tube outer diameter constitutes a wetted surface. Limited sensitivity studies have been performed to determine the effect of applying the crevice pressure over a smaller portion of the tube. In these studies, “bubbles” of crevice pressure were applied to the tube bore inner diameter and the tube outer diameter while the full internal pressure was applied to the inner diameter of the tube. The “bubbles” varied in circumferential extent from 10 to 75 percent of the tube outer diameter. The effect of limiting the crevice pressure to less than 100 percent of the outer tube diameter was an increase in the average tube to tubesheet contact pressure of at least 10 percent.

## 2.4 DISCUSSION OF MATERIAL PROPERTIES

The manufacturing process used to assemble a steam generator creates a strain hardened condition in the tubes. The tubes are initially inserted into the steam generator tubesheet tube bores, “tack” expanded into the tubesheet near the tube end by hydraulic (urethane plug) expansion or mechanical hard rolling over approximately a 0.75 inch length, and welded to the tubesheet. Each tube is then hydraulically expanded into contact with the tubesheet tube bore over the full depth of the tubesheet. This means that each of the tubes in the tube bundle begins in contact with the tubesheet tube bore. It also means that the tubes create a material non-linearity with respect to the contact pressure analysis because they are strain hardened to a small percentage (1 to 3 percent on average) and typically thinned to a small extent (~1 percent wall thinning). No non-linear material effects are present in the tubesheet tube bore material. Consistent with the basis of the current licensing basis, the square cell model ignores any effects that could benefit the contact pressure analysis that come from the tube installation and steam generator manufacturing process, including any strain hardening effect, residual contact pressure, wall thinning, or other material non-linearity.

Test data has shown that the installation and tube expansion process develops sufficient pull out resistance between the tube and the tubesheet at room temperature and at elevated temperature conditions (References 2-1 and 2-2) to resist any applied pull out loads during normal and accident conditions. Any additional contact pressure due to tubesheet deformation or applied pressure is above and beyond what is already sufficient to prevent pull out of the tube portion within the tubesheet. Therefore, it is conservative and convenient to ignore strain hardening resulting from initial tube expansion as an initial condition. No elastic-plastic effects are included in the analysis. The displacements and pressures acting on the tubes are applied in an elastic analysis. This is appropriate provided that the average radial stress in the tube material due to the applied loads is less than  $[ ]^{a,c,e}$  ksi. None of the contact pressure results in the tube material for the square cell model described in this report approached an average radial stress of  $[ ]^{a,c,e}$  ksi.

The material properties used for the tube and the tubesheet materials in square cell model are the same as originally used in the licensing basis analysis, References 2-1 and 2-2. The properties used for the Alloy 600 thermally treated tubing and SA-508 tubesheet materials are provided in Tables 3-2 and 3-4.

The Poisson's Ratio used for the tube material is [ ]<sup>a,c,e</sup>. The Poisson's Ratio used for the tubesheet material is [ ]<sup>a,c,e</sup>.

## 2.5 CONTACT MODELING DISCUSSION

The only boundary conditions that limit the displacement of the tube in the square cell model are the symmetry conditions on the edges of the model. This means that in the square cell model the contact between the tube and the tubesheet is what limits the potential displacement of the tube. If the contact relationship between the tube and the tubesheet is modeled inappropriately, the tube in the model could slide past the tubesheet and experience rigid body translation. Another possibility is that the tube deformations could lead to inter-penetration of the tube material into the tubesheet material which would generate unrealistically high contact pressures. Conversely, if the contact law is determined to resist node to node contact too strongly, the results of the analysis would be an unrealistically low contact pressure. While the *ANSYS* solver is capable of using different numerical schemes to resolve these difficulties, it is up to the user to make sure that the results which are obtained are appropriate. In the application of the square cell model, the contact pressure results using different contact modeling options were compared to determine the best approach. The final contact model used in the square cell analysis is a frictional model which is consistent with the assumptions in the  $H^*$  analysis (e.g.,  $\mu = [ ]^{\text{a,c,e}}$ ).

The simplest way to prevent difficulties with a contact law is to construct a properly converged mesh. It is difficult for nodal interpenetration to occur if a mesh is fine enough, and the nodal positions on either side of the contact interface are aligned properly. Two mesh designs were evaluated in the  $C^2$  analysis. Figure 2-8 shows the two meshing schemes of the model used in the analysis. The coarse mesh (shown in Figure 2-8a) has approximately [ ]<sup>a,c,e</sup> contact elements along the tube-to-tube bore interface. The fine mesh (shown in Figure 2-8b) has approximately [ ]<sup>a,c,e</sup> contact elements along the tube-to-tube bore interface. The fine mesh tends to predict an increase in the tube-to-tubesheet contact pressure relative to the coarser mesh and can resolve the contact pressure closest to the boundaries in a quarter symmetry model. However, the contact pressures nearest the displacement boundary conditions on the tube in the quarter symmetry model are not significant to the problem and lower contact pressures are conservative. Therefore, for conservatism, the preferred meshing scheme in the square cell analysis is a more coarse mesh. The actual mesh used in the final analysis is a slightly less coarse mesh than that shown in Figure 2-8a.

The tubesheet is defined as the contact target body because the deformation of the tubesheet material is more controlled. The tube is defined as the contact body because the tube is expanding into the tubesheet material and its deformation is poorly controlled in the model. The contact relationship between the tube and the tubesheet is defined as symmetric and rough (e.g., with friction). The contact is symmetric for numerical expediency and because, in the range of deformations under consideration, the tube may lose contact with the tubesheet or the tubesheet may lose contact with the tube. The friction interface allows two-dimensional sliding between the tube and the tubesheet. Shear stresses can develop due to "stick-slip" behavior because the coefficient of friction between the tube and the tubesheet in this model is greater than zero. However, these shear stresses are separate from the calculated contact pressures in *ANSYS* and do not affect the final results used to calculate  $H^*$ .

The augmented Lagrangian solver in *ANSYS* is used to resolve the contact so that the contact pressure results have a smaller variation around the circumference of the tube bore and because the extra degree of

freedom helps the solver to calculate the contact interactions quickly. The tube and tubesheet are initially adjusted to be “just touching” using the contact options in *ANSYS*. The geometry defined in the model is such that the tube and tubesheet begin in line on line contact at the tube-to-tubesheet interface. However, the possibility exists for a small geometric inconsistency to lead to an interpenetration of the tube and tubesheet materials. Therefore, the tube outer surface and tubesheet inner surface are separated by an initial offset of +0E00 inch in *ANSYS* to set the initial gap to zero and to assure that no interpenetration occurs. There are two options used in the analysis for managing the stiffness of the interface in the square cell model. The first option assumes that the stiffness of the interface is constant and does not need to be updated as the analysis proceeds to completion. This first option is the most similar to an analytical model using thick shell equations to solve for the contact pressure between the tube and the tubesheet. The second option assumes that the stiffness must be constantly updated to prevent interpenetration of the tube and tubesheet and adjust the contact law as the deformation of the nodes at the interface shift during the analysis. The “pinball” radius, the radius about a node in which, if another existing node is recognized to be in contact, was set to [ ]<sup>a,c</sup> inch to reflect the surface roughness of the post-expanded tube.

## 2.6 DISCUSSION OF BENCHMARK MODEL FOR C<sup>2</sup> MODEL COMPARISON

The contact pressure results for the square cell analysis were benchmarked against classical thick shell equations. The thick shell model for the composite tube and tubesheet collar was developed to accept the displacement of the tubesheet inner diameter surface as input. The benchmark model used the Model D5 tube and tubesheet geometry; therefore, the temperature and geometry information in this section may be different than the similar information that applies to the Model 44F and 51F steam generators. However, the conclusions based on this benchmarking process are applicable to all models of SG. The benchmark model used a different thick shell model (see below) than described in the existing licensing basis for the calculation of the H\* analysis contact pressures because the goal of the model was to provide an independent check on the square cell model results and the H\* methodology.

### 2.6.1 Thick Shell Model to Describe Finite Element Model

The tube and tubesheet cylinders can be represented as two concentric, open cylinders. The tube material is thermally treated Alloy 600. The tubesheet material is SA-508 Class 2. Neither cylinder has an applied axial load. There is no internal pressure within the tube. The coefficient of friction between the inner diameter of the tubesheet and the outer diameter of the tube is zero. The tube and the tubesheet are held at the same constant temperature during the simulation of the operating condition although the tubesheet is assumed to have a coefficient of thermal expansion equal to zero. The tube bore dilation, or expansion of the inner tubesheet collar diameter, is specified in the analysis and assumed to be constant regardless of any applied loading for the tube. The tube and tubesheet cylinders are assumed to have a zero stress, or a constant stress condition, along the tube axis (e.g.,  $\sigma_{zz} = 0$  psi). The assembled model geometry appears in Figure 2-10.

In Figure 2-10,  $a$  is the inner radius of the tube,  $b$  is the outer radius of the tube and also the inner radius of the tubesheet tube bore, and  $c$  is the outer radius of the tubesheet collar.

The free radial expansion of the tube, due to a change in temperature, is given by:

$$\Delta R_{\Delta T} = \frac{OD}{2} \cdot \alpha_{TUBE} (t - t_{REF}) \quad (\text{Equation 2-1})$$

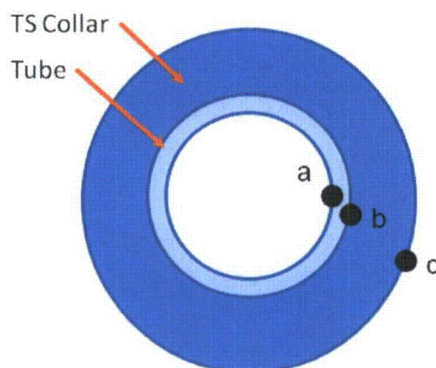


Figure 2-10 Tube and TS Collar Assembly.

Where OD is the outer diameter of the tube,  $\alpha_{TUBE}$  is the coefficient of thermal expansion of the tube,  $t$  is the temperature of the tube and  $t_{REF}$  is the reference temperature in the analysis for the material of interest (typically 70°F). Several values of constant tubesheet tube bore inner diameter displacements were selected for the purposes of this sensitivity study. It is assumed that the tubesheet is essentially rigid with respect to any applied loading from the tube in excess of the initial dilation. The tube bore is assumed to deform (or dilate) as a perfect circular surface without any non-uniformities around the circumference of the tube. The difference between the specified tubesheet tube bore dilation and the amount that the tube wants to expand will create a contact stress between the tube and the tubesheet (see Figure 2-11).

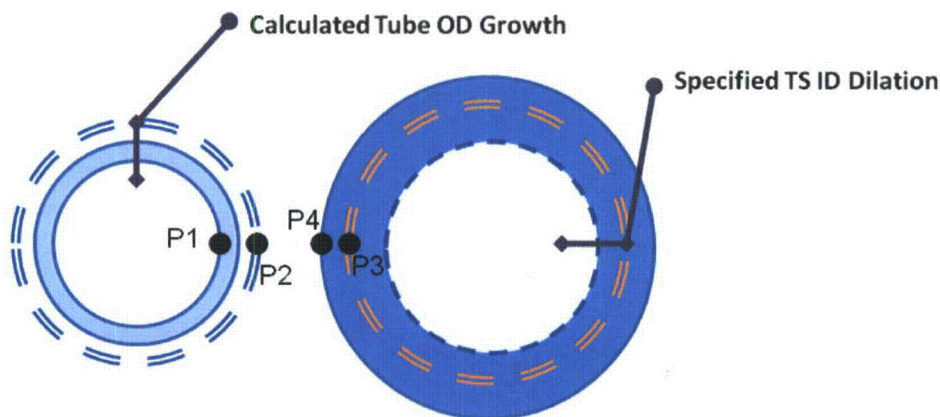


Figure 2-11 Constant Tubesheet Bore Dilation Model

In Figure 2-11, P1 is the internal pressure applied to the inner surface of the tube, P2 is the external pressure applied to the outer surface of the tube, P3 is the internal pressure applied to the inner surface of the tubesheet collar, and P4 is the external pressure applied to the outer surface of the tubesheet collar. In the tube and tubesheet assembly, the contact pressure between the two cylinders is taken at the inner surface of the tubesheet collar and the outer surface of the tubesheet such that they are both equivalent (e.g., P2 = P3). There are no other applied pressures on the system so P1 = P4 = 0 psi.

The differential free radial expansion of the tube at normal operating conditions (NOP,  $t = [ \quad ]^{a,c,c} \text{ } ^\circ\text{F}$ ) and steam line break conditions (SLB,  $t = [ \quad ]^{a,c,c} \text{ } ^\circ\text{F}$ ) is calculated using Equation 2-1 and the material properties defined in Table 3-3 and Table 3-4. The NOP operating temperature of  $[ \quad ]^{a,c,c} \text{ } ^\circ\text{F}$  was chosen to better compare to previous results in Reference 2-7 and is still representative of typical NOP conditions. The results are summarized in Table 2-1.

The difference between the inward radial dilation of the tubesheet tube bore and the outer diameter of the tube will change based on the temperatures during operation. The difference between the specified radial dilation of the tubesheet tube bore and the radial growth of the tube for each operating condition is shown in Table 2-2.

Column (1) in Table 2-2 is the assumed inner radius of the tubesheet tube bore and Column (2) in Table 2-2 is the amount that the tubesheet tube bore is allowed to dilate in the analysis. Column (3) and Column (4) in Table 2-2 are the difference between the allowed dilation in Column (2) and the results in Table 2-2 for each operating condition (e.g.,  $\Delta U_{\text{NOP}} = \text{Tube Growth} - \text{Tubesheet Growth}$ ). The difference between the deformations is taken so that a positive value means that the tube deformation exceeds the growth allowed by the tubesheet collar

The equation for the radial deformation (either positive or negative) of the tube as an open thick walled cylinder at a constant temperature due to pressure loading is:

$$\Delta R_{\text{TUBE}} = \frac{r}{E_{\text{TUBE}}(b^2 - a^2)} \left[ (1 - \nu_{\text{TUBE}})(p_1 a^2 - p_2 b^2) + \frac{(1 + \nu_{\text{TUBE}})a^2 b^2}{r^2} (p_1 - p_2) \right] \quad (\text{Equation 2-2})$$

Where  $r$  is the radial location within the tube material,  $b$  is the outer radius of the tube,  $a$  is the inner radius of the tube,  $E_{\text{TUBE}}$  is the Young's modulus of the tube at the given operating condition and  $\nu_{\text{TUBE}}$  is the Poisson's Ratio for the tube material. The equation for the radial deformation (either positive or negative) of the tubesheet collar as an open thick walled cylinder at a constant temperature due to pressure loading is:

$$\Delta R_{\text{TS}} = \frac{r}{E_{\text{TS}}(c^2 - b^2)} \left[ (1 - \nu_{\text{TS}})(p_3 b^2 - p_4 c^2) + \frac{(1 + \nu_{\text{TS}})b^2 c^2}{r^2} (p_3 - p_4) \right] \quad (\text{Equation 2-3})$$

Where  $r$  is the radial location within the tubesheet material,  $c$  is the outer radius of the tubesheet collar,  $b$  is the inner radius of the tubesheet collar,  $E_{\text{TS}}$  is the Young's modulus of the tubesheet at the given operating condition and  $\nu_{\text{TS}}$  is the Poisson's Ratio for the tubesheet material.

The deformation of the tube is limited by the specified deformation of the tubesheet collar, as shown in Table 2-2, Columns (3) and (4). The values in Columns (3) and (4) are all positive, therefore, the final state of the tube outer surface and the tubesheet inner surface is positive contact. The magnitude of the contact pressure between the tube and the tubesheet will be the result of the additional growth that the tube cannot release due to the “rigid” tubesheet collar. The equation for the change in radial position of the contact surface between the tube and the tubesheet is:

$$\Delta U = [\Delta R_{TS}]_{r=b} - [\Delta R_{TUBE}]_{r=b} \quad (\text{Equation 2-4})$$

Where  $\Delta U$  is the condition specific result from Table 2-2 for the appropriate value of tubesheet collar dilation in Column (2). Setting P1 and P4 equal to zero and P2=P3 in Equation 2-2 and Equation 2-3 yields the following for  $r = b$ ,

$$\begin{aligned} \Delta U = & \frac{b}{E_{TS}(c^2 - b^2)} \left[ (1 - \nu_{TS})(p_2 b^2) + \frac{(1 + \nu_{TS})b^2 c^2}{b^2} (p_2) \right] - \dots \\ & \dots - \frac{b}{E_{TUBE}(b^2 - a^2)} \left[ (1 - \nu_{TUBE})(-p_2 b^2) + \frac{(1 + \nu_{TUBE})a^2 b^2}{b^2} (-p_2) \right] \end{aligned} \quad (\text{Equation 2-5})$$

Rearranging to solve for P2 gives the final result.

$$p_2 = \Delta U \left[ \frac{b}{E_{TS}(c^2 - b^2)} \left[ (1 - \nu_{TS})(b^2) + (1 + \nu_{TS})c^2 \right] + \frac{b}{E_{TUBE}(c^2 - b^2)} \left[ (1 - \nu_{TUBE})(b^2) + (1 + \nu_{TUBE})a^2 \right] \right]^{-1} \quad (\text{Equation 2-6})$$

In this case the contact pressure is a kind of residual stress locked into the assembly by the restrictions on tube deformation.

Solving Equation 2-6 for each value in Column (3) and Column (4) in Table 2-2 with the properties in Table 2-3 and Table 2-4 yields the results shown in Table 2-5.

The results in Table 2-6 exclude any effect of non-uniform deformation around the circumference of the tubesheet tube bore. The loss of contact pressure between the tube and the tubesheet is due solely to the expansion (or dilation) of the tubesheet tube bore relative to the expansion of the tube due to thermal effects. Real deformations applied to the tubesheet tube bore are not perfectly uniform. Therefore, the displacement of the inner tubesheet tube bore was used in order to benchmark the model to compare directly against the C<sup>2</sup> model. Only the average tube to tubesheet contact pressure around the circumference of the tube can be calculated using the thick shell equation. This is an acceptable comparison to the finite element results because only the average contact pressure around the circumference of the tube is used in the calculation of H\*. This benchmark was performed for the Model D5 NOP condition. The expansion of the inner surface of the tubesheet tube bore due to a pressure differential across the tube wall (i.e., the pressure of the primary fluid minus the assumed circumferentially uniform pressure in the tube/tubesheet crevice) and an applied temperature is shown in Table 2-6. This result was then applied to the inner diameter of the tubesheet surface in the C<sup>2</sup> model. The tube bore displacement in Table 2-6 varies as a function of elevation due to the change in the crevice

pressure distribution. The result of using the calculated tubesheet tube bore displacements in the square cell and analytical models is given in Table 2-7. The average contact pressure between the tube and the tubesheet in the  $C^2$  approach with the contact law as described is a very close approximation of the thick shell equation for the same uniform tubesheet tube bore displacement. Based on the comparison with the thick-shell equation models, the  $C^2$  approach and the modeling described in this section are reasonable and appropriate.

**Table 2-1 Free Radial Expansion of a Tube**

Condition	Nominal Tube OR	$\alpha_{TUBE}$	T	$t_{REF}$	$\Delta R$
	in	in/in-°F	°F	°F	in
NOP					
SLB					

a,c,e

Note: Benchmarking analysis was based on Model D5 geometry and conditions.

**Table 2-2 Difference Between Radial Dilatation of the Tube Bore and Tube**

(1)	(2)	(3)	(4)
Avg TS IR	Change in TS IR	$\Delta UNOP$	$\Delta USLB$
in	in	in	in

a,c,e

Note: Benchmarking analysis was based on Model D5 geometry and conditions.

**Table 2-3 Rigid Collar Model Input Parameters (Tube)**

Nominal Tube Properties			
Variable	Description	Value	Units
b	OR		in
a	IR		in
	E (NOP)		psi
	E (SLB)		psi
	$\alpha$ (NOP)		in/in-°F
	$\alpha$ (SLB)		in/in-°F
	Poisson's Ratio		-

Note: Benchmarking analysis was based on Model D5 geometry and conditions.

**Table 2-4 Rigid Collar Model Input Parameters (Tubesheet)**

Nominal TS Properties			
Variable	Description	Value	Units
c	OR		in
b	IR		in
	E (NOP)		psi
	E (SLB)		psi
	a (NOP)		in/in-°F
	a (SLB)		in/in-°F
	Poisson's Ratio		-

Note: Benchmarking analysis was based on Model D5 geometry and conditions.

**Table 2-5 Rigid Collar Model Contact Pressure Results**

(1)	(2)	(3)	
Avg. TS IR	P2 NOP	P2 SLB	
In	Psi	psi	a,c,e
0.3810			
0.3811			
0.3813			
0.3815			

**Table 2-6 Calculated Tubesheet Inner Diameter Dilation**

Thermal Expansion of TS ID		[ ] <sup>a,c,e</sup>	in
Tubesheet Elevation	$\Delta P_{CREV}$ Expansion	Combined Expansion <sup>a,c,e</sup>	
BTS			in
NA			in
TTS			in

Note: Benchmarking analysis was based on Model D5 geometry and conditions.

**Table 2-7 Comparison of C<sup>2</sup> and Thick Shell Results**

	Contact Pressure Results			a,c,e
	TTS	NA	BTS	
Max (psi)				
Min (psi)				
Average (psi)				
Thick Shell				

---

## 2.7 REFERENCES

- 2-1. WCAP-17091-P, Revision 0, "H\*: Alternate Repair Criteria for the Tubesheet Expansion Region in Steam Generators with Hydraulically Expanded Tubes (Model 44F)," June 2009.
- 2-2. WCAP-17092-P, Revision 0, "H\*: Alternate Repair Criteria for the Tubesheet Expansion Region in Steam Generators with Hydraulically Expanded Tubes (Model 51F)," June 2009.
- 2-3. *Stress Analysis of Thick Perforation Plates*, T. Slot, 1972.
- 2-4. LTR-SGDA-07-4 (Proprietary), "Letter Summary of Changes to B\* and H\* Analysis due to New Crevice Pressure and Divider Plate Data," Westinghouse Electric Company LLC, Pittsburgh, PA, January 17, 2007.
- 2-5. STD-MC-06-11-P, Rev. 1, "Pressure Profile Measurements During Tube-to-Tubesheet Leakage Tests of Hydraulically Expanded Steam Generator Tubing," Westinghouse Electric Company LLC, Pittsburgh, PA, August 30, 2007.
- 2-6. *Journal of Pressure Vessel Technology*, August 2006, Volume 128, Issue 3, pp 408-413.
- 2-7. WCAP-17072-P, Revision 0, "H\*: Alternate Repair Criteria for the Tubesheet Expansion Region in Steam Generators with Hydraulically Expanded Tubes (Model D5)," May 2009

---

### 3 STRUCTURAL CALCULATIONS FOR H\*

Section 2 of this report provided a general description of the  $C^2$  model, its intent, its design, how it fits in the overall process for calculating the  $H^*$  distance, and what its capabilities are relative to the thick-shell equation model. This section summarizes the application of the 3-D FEA and  $C^2$  models to the Model 51F and 3-loop Model 44F SGs. Sections 3.1 through 3.3 summarize the significant assumptions in the application of the  $C^2$  model, and the interface between the  $C^2$  model and the 3-D FEA model of the lower tubesheet complex. Section 3.2 discusses the boundary conditions applied for the only Model 51F plant, Surry Units 1 & 2, and the boundary conditions applied for the limiting Model 44F plant, Turkey Point Units 3 & 4. Except for detailed geometry, the application of the 3-D FEA model is the same for both the Model 51F and Model 44F SGs. Therefore, the figures provided are to be taken as generic results, applicable to both the Model 51F and Model 44F SGs, although the figure titles refer to the specific analysis from which they were taken. Section 3.3 discusses the solution for the mean value of  $H^*$  based on application of the  $C^2$  model, including the displacement inputs from the 3-D FEA model and the axial contact pressure profiles each tubesheet radius for both the Model 51F and Model 44F SGs in both tabular and graphical form. Section 3.4 provides the probabilistic analysis based on the  $C^2$  model for the Model 51F and Model 44F SGs. By its design and its interface with the 3-D FEA model of the lower tubesheet complex, the  $C^2$  model cannot directly include the effect of Poisson contraction on  $H^*$ ; however, Section 3.5 provides the analysis of Poisson contraction on  $H^*$  predicted using the  $C^2$  model. In this section, Surry Units 1 & 2 and Turkey Point Units 3 & 4 are frequently discussed. Surry Units 1 & 2 are the only Model 51F SG plants and Turkey Point Units 3 & 4 are the identical limiting plants for the Model 44F SG plants. The criteria for defining the limiting plants are discussed in the current licensing basis (i.e., References 3-1 and 3-2).

#### 3.1 OVERVIEW OF THE STRUCTURAL ANALYSIS FOR H\*

As noted in Section 2.0 of this report, the  $C^2$  model is a planar model of a tube in a tubesheet segment. The tubesheet segment can be visualized as a square local segment of the tubesheet that is defined by a single tube pitch ([ ]<sup>a,c,c</sup> inches for the Model 51F, [ ]<sup>a,c,c</sup> inch for the Model 44F) centered on the location of a tube (see Figure 2-4). The model includes the tubesheet bore and a tube in its expanded diameter but without any residual contact pressure from the hydraulic expansion process. Thus, in its unloaded state, the tube is in zero-pressure line-on-line contact with the tubesheet bore.

The loading conditions applied to the square cell model are:

- temperature, which varies axially through the tubesheet
- the internal tube pressure modified by the axially-dependent crevice pressure
- planar displacements at the model boundaries, which are taken from the 3-D-FEA model of the tubesheet complex when it is loaded by temperature increase and differential pressures applicable to the operating conditions of interest

In the licensing basis analysis, when applying the thick-shell model, similar displacements were applied directly to the tubesheet bore; however, in the  $C^2$  model application, the displacement conditions are

---

applied to the boundaries of the model and the model determines the conditions at the actual tube-to-tubesheet interface. This is a key difference between the  $C^2$  model and the thick shell model.

To calculate the axial contact pressure profile for a tube at the tubesheet radius of interest, the temperatures and displacements appropriate to nine points through the thickness of the tubesheet are input separately to the model along with the tube-wall pressure differential between the internal pressure of the tube, and the crevice pressure acting on the outer diameter of the tube wall and inner diameter of the tubesheet applicable to each elevation to determine the contact pressure between the tube and the tubesheet at each elevation. The elevations through the thickness of the tubesheet are consistent with the elevations utilized in the current licensing basis for  $H^*$ . Application of the  $C^2$  model assumes that the centerline of the tube remains straight, e.g., that no bending of the tubesheet occurs. The displacement input conditions, taken from the 3-D FEA model of the tubesheet complex, include the total effects of temperature and pressure loading in the continuum of the thickness of the tubesheet. Ignoring the coupling due to tubesheet bending in applying the  $C^2$  model is a very conservative application of this model because the introduction of tubesheet bore and tube bending would be expected to result in much higher contact pressures between the tube and tubesheet.

The input boundary conditions include displacements in both axes of the plane. Conceptually, this is similar to the original analysis using the thick-shell equations, but the application details are different. Previously, the radial displacement was taken directly from the 3-D FEA model, and the circumferential displacement was derived from the radial displacement (see Section 6.3 of References 3-1 and 3-2) and applied directly to the tubesheet bore. For application of the  $C^2$  model, which is driven by the cell boundary displacements, it was desired that the radial displacements be calculated directly in the 3-D FEA model of the tubesheet complex. To facilitate this, the 3-D-FEA model was modified by adding the same mesh used on the tubesheet centerline face perpendicular to the divider plate one and two pitches into the depth (not thickness) of the tubesheet. This permitted obtaining the displacements in the direction parallel to the divider plate directly from the 3-D FEA model for application to the  $C^2$  model boundaries instead of direct application to the tubesheet bore.

The 3-D FEA model mesh was also modified for other reasons not directly related to application of the  $C^2$  model. For example, to avoid applying a factor to account for a non-functional divider plate, the model was changed to directly reflect that the upper five inches of the divider plate were assumed to be non-existent (see Section 3.2.2). Further, changes were made to the 3-D FEA model mesh to properly represent the axial thermal profile through the thickness of the tubesheet (see Section 3.2.5).

## **3.2 STRUCTURAL ANALYSES (3-D FEA MODEL)**

### **3.2.1 Method Discussion**

The structural finite element analysis is based on a 3-dimensional (3-D) model of the lower steam generator complex consisting of the channelhead, divider plate, tubesheet, and lower shell. The model uses Slot's effective material properties to model the perforated tubesheet section as an orthotropic material, as discussed in References 3-3, and 3-4. The plants are analyzed for low  $T_{avg}$  normal operating conditions (NOP) and steam line break (SLB), which have been determined to be limiting conditions in References 3-3 and 3-4. Note that these conditions represent the bounding pressure and temperature.

---

values specified by the design basis transients and represent the design limits of the plant operating conditions but not the current actual plant operating conditions.

### 3.2.2 Discussion of Significant Assumptions

The assumptions below, with the exception of the thermal temperature profile through the tubesheet, are copied from References 3-1 and 3-2. For each analysis condition, a thermal and a combined thermal-structural analysis were performed to determine the deformations in the tubesheet. All of the finite element analysis (FEA) results assume a static, steady-state, linear, and elastic system.

An analysis performed in Reference 3-3 concludes that, in general, the tubesheet is approximately at the primary side temperature through its thickness, except for a sharp thermal gradient that exists in approximately the top one (1.00) inch. In the thermal analysis, the secondary side of the tubesheet was assumed to be at a temperature equal to the average of the steam temperature and the feedwater temperature. The tubesheet portion of the 3-D FEA model used in this analysis was partitioned two (2.00) inches from the top of the tubesheet. From the bottom of the tubesheet to the top of this partition in the tubesheet, an approximately uniform temperature equal to the hot leg temperature was applied. This produced a temperature gradient in the top two inches of the tubesheet from a value of 10 degrees cooler than the primary fluid temperature to the average of the coldest allowable condition-specific feedwater and steam outlet temperatures as specified by the applicable PCWG (see Section 5 of References 3-3 and 3-4 for details). For the SLB case, the primary fluid and the average of the secondary fluids were applied to the primary and secondary surfaces of the tubesheet, respectively, so that a linear temperature gradient developed through the thickness of the tubesheet. This is a reasonable assumption because the long-term portion of the transient specifies that flow will be reduced to natural circulation through the affected loop when the reactor coolant pumps are off.

Where a range of feedwater temperatures was specified in the PCWG parameters, the condition most conservative for  $H^*$  was used. Since  $H^*$  values are negatively impacted (i.e., greater  $H^*$  values result) by large radial deformations of the tubesheet, a higher overall temperature of the tubesheet will result in a lower modulus, and thus a conservative  $H^*$  value. Note that only the tubesheet temperature is at issue here because the tube temperature remains at the design  $T_{hot}$  for the normal operating condition.

The transient analyses for SLB are performed statically. This results in a conservative  $H^*$  value, because the maximum pressure and asymptotic temperature from the transient is used. It is reasonable to use a static analysis for the long-term conditions since these transients are very long and the steady-state portion of the transient continues for hours.

The dimensions used for the finite element model were consistent with the current licensing basis.

The finite element model did not include the nozzles or manways. This is reasonable because the deformations of interest are in the tubesheet, which is well removed from the channelhead penetrations, and thus, would not be expected to have a significant effect on tubesheet deflections. Prior analysis has shown that including the larger channelhead penetrations, such as the manways, tends to decrease displacements in the tubesheet. Decreasing tubesheet displacements will produce shorter  $H^*$  distances; therefore, the current approach is conservative. The model did not consider the tubes or any of the structure above the tubesheet except the lower shell (stub barrel). Including the portion of the tube within

the tubesheet decreases the tubesheet displacement because it stiffens the tubesheet with respect to the bending caused by the primary-to-secondary pressure differential (Reference 3-7).

The upper five inches of the divider plate, stub runner, and weld material is suppressed in the analysis of the combined thermal and pressure load cases to address concerns from the Nuclear Regulatory Commission regarding the potential for divider plate cracking. This condition is discussed in Reference 3-4, which details the assessment of a fully degraded divider plate to tubesheet weld in terms of the divider plate factors discussed in References 3-1 and 3-2. In the current analysis, a variant of the 3-D FEA lower tubesheet complex model was created that excluded the upper five inches of the divider plate and application of this model directly confirmed the conclusions of References 3-1 and 3-2 that this assumption is conservative relative to H\*.

### 3.2.3 Input

The input for this analysis consists of steam generator dimensions for the plants to be analyzed, material properties from the ASME code, and pressure and temperature conditions from the PCWG parameters and transients as documented in References 3-1 and 3-2.

The input boundary conditions for the limiting plants are Table 3-1 and Table 3-2 for the Model 51F plants and Model 44F plants, respectively. The modulus of elasticity and coefficients of thermal expansion are provided in Table 3-3 and Table 3-4. The tubesheet is SA-508 Class 2A, the divider plate is Alloy 600 (SB-168), the channelhead is SA-216 grade WCC, and the lower shell is SA-533 Grade A Class 2. These are the same values included in References 3-3 and 3-4.

### 3.2.4 Geometry

The geometry analyzed for the Model 51F and 44F SGs is essentially identical to that considered in the baseline analyses in References 3-3 and 3-4. The only modifications were the addition of several model partitions in the tubesheet region and truncating the divider plate. The first partition in the tubesheet model is at two inches from the secondary surface to accommodate a non-linear temperature profile. Additional solid body partitions were made through the tubesheet at distances equal to one and two pitches behind the half-symmetry plane to facilitate the post-processing of displacements for the square cell model. The typical solid models used are shown in Figure 3-1 for the Model 51F SGs (Surry Units 1 & 2) showing the truncated divider plate and Figure 3-2 for the Model 44F SG (Turkey Point Units 3 & 4) showing the model with the complete divider plate.

For the current H\* analysis, the upper five inches of the divider plate, stub runner and weld material is suppressed in the analysis of the combined thermal and pressure load cases. This approach, used to avoid potential concerns regarding cracking of the divider plate was shown in prior analysis to be conservative for H\* References 3-3 and 3-4, Section 6.2.6. Figure 3-1 shows a typical representation of the solid body with the upper five inches of the divider plate and attached materials suppressed. Eliminating this material in the model does not change the application or values of the applied boundary conditions nor does it change the results of the thermal analysis. The only effect that truncating the divider plate has is that the tubesheet has less resistance to the applied pressure loads than if it were connected to the divider plate. However, the steam generator model with the severed divider plate is the same model as the steam generator with an intact divider plate in all other respects.

---

### 3.2.5 Mesh Discussion

In general, the model meshes for all models of SG among the H\* candidate population are similar but are adjusted to accommodate the specific geometry of each model of SG. The model meshes used in the analyses for the Model 51F and Model 44F SGs are essentially the same as the mesh documented in References 3-1 and 3-2. Additional constraints were added to the current mesh to accommodate the vertical partition through the tubesheet. The typical mesh used is shown in Figure 3-3, Figure 3-4, and Figure 3-5 for the principal axes.

### 3.2.6 Tubesheet Equivalent Properties

Modeling of the equivalent properties of the perforated plate (tubesheet) by the method of Slot is discussed in Section 6.2.1 of References 3-3 and 3-4. The same equivalent properties used in References 3-3 and 3-4 were used in the current analysis. Information from those references is included here for completeness. Interpolated ratios of equivalent properties are in Table 3-5, where the "\*" indicates the properties of the equivalent tubesheet. The ratios are then multiplied by the material properties for SA-508 Class 2A in Table 3-3 to obtain the temperature-dependent equivalent properties. The equivalent properties for the tubesheet are in Table 3-6 and Table 3-7 for the Model 51F SG and Model 44F SG, respectively.

### 3.2.7 Boundary Conditions

The application of the boundary conditions to the models is consistent with those included in the current licensing basis, Reference 3-1 and Reference 3-2. Table 3-1 and 3-2 summarize the specific boundary conditions and how they are applied to the 3-D-FEA model. Two different analyses were performed with the 3-D FEA model of the lower SG tubesheet complex to support application of the C<sup>2</sup> model:

1. Thermal Analysis: The operating temperature conditions only were applied to the SG, with a reference temperature of 70°F. The result from this analysis is purely a temperature profile through the tubesheet.
2. Deflection Analysis: In this analysis, the non-uniform temperature profile from the first analysis and the pressure loads are simultaneously applied to the model. The results from this analysis, with the severed divider plate condition, are used in the final H\* analysis. Instead of accounting for the absence of the divider plate by application of a divider plate factor, as in the licensing basis analysis. All of the required displacements and effects are directly accounted for by ANSYS.

The results of the second analysis provide the input for subsequent analysis with the square cell model which replaces the thick shell model in the current licensing basis. The approach in the second analysis is beneficial because it eliminates the need to separately post-process and calculate the different displacements required for the H\* analysis, as was done in the licensing basis.

The applied loads and temperatures in each analysis are shown in Table 3-1 and Table 3-2. The analysis was applied only to the limiting conditions required for H\*; that is, if a plant's limiting H\* distance is

---

controlled by the normal operating (NOP) condition, the NOP pressures and temperature loads were used in the analysis and the SLB conditions were not considered and vice versa.

### **3.2.8 Tubesheet Complex 3-D FEA Analysis Results**

This section provides typical results of the 3-D FEA analysis. The figures discussed in this section are taken from the analysis of the Model 51F SG, but are generic in nature. Except for SG geometry difference, there are no significant differences in the analysis for the Model 44F SGs. Typical results of the thermal analysis for normal operating conditions are shown in Figure 3-6. The thermal profile is slightly different than that in the licensing basis document, but is more accurate due to the direct application of temperature loads to the tubesheet partition. Figures 3-7 through 3-9 show the results of the thermal-structural analysis for Surry for 100 percent power. Figure 3-10 shows the results of the SLB thermal analysis for Surry. Aside from the severed divider plate, these results are the same as in the licensing basis. Figures 3-11 and 3-12 show the X- and Z-deformations for SLB for Surry Units 1 and 2. The results of the current 3-D FEA, as documented in this report, are taken from Reference 3-6.

**Table 3-1 Input Boundary Conditions for Model 51F (Surry)**

Parameter	Low $T_{avg}$	SLB	
Hot Leg Pressure (psia)	[	]	a,c,e
SG Outlet Pressure (psia)			
Secondary Pressure (psia)			
Hot Leg Temperature (°F)			
SG Outlet Temperature (°F)			
Steam Temperature (°F)			
Feedwater Temperature (°F)			
Mean Shell Radius $r_m$ (inches)			
Shell Thickness $t$ (inches)			
<b>Calculated Values</b>			
Secondary Fluid Temperature	[	]	a,c,e
Endcap Load (psia)	[	]	

**Table 3-2 Input Boundary Conditions for Model 44F (Turkey Point)**

Parameter	Low $T_{avg}$	SLB	
Hot Leg Pressure (psia)	[	]	a,c,e
SG Outlet Pressure (psia)			
Secondary Pressure (psia)			
Hot Leg Temperature (°F)			
SG Outlet Temperature (°F)			
Steam Temperature (°F)			
Feedwater Temperature (°F)			
Mean Shell Radius $r_m$ (inches)			
Shell Thickness $t$ (inches)			
<b>Calculated Values</b>			
Secondary Fluid Temperature	[	]	a,c,e
End cap Load (psia)	[	]	

**Table 3-3 Modulus of Elasticity for Materials**

Temperature (°F)	SA-508 Class 2A (Msi)	Alloy 600 (Msi)	SA-216 Grade WCC (Msi)	SA-533 Grade A Class 2 (Msi)
70	29.2	31.0	29.5	29.2
200	28.5	30.2	28.8	28.5
300	28.0	29.9	28.3	28.0
400	27.4	29.5	27.7	27.4
500	27.0	29.0	27.3	27.0
600	26.4	28.7	26.7	26.4
700	25.3	28.2	25.5	25.3

**Table 3-4 Coefficient of Thermal Expansion for Materials**

Temperature (°F)	SA-508 Class 2A (µin/in)	Alloy 600 (µin/in)	SA-216 Grade WCC (µin/in)	SA-533 Grade A Class 2 (µin/in)
70	6.50	6.90	5.53	7.06
200	6.67	7.20	5.89	7.25
300	6.87	7.40	6.26	7.43
400	7.07	7.57	6.61	7.58
500	7.25	7.70	6.91	7.70
600	7.42	7.82	7.17	7.83
700	7.59	7.94	7.41	7.94

**Table 3-5 Interpolated Ratios of Equivalent Material Properties for Analysis of Perforated Plate**

Property	Model 51F	Model 44E	a,c,e
Gy*/ Gy			
Ey*/ Ey			
Ep*/ Ep			
Gp*/Gp			
Poisson's Ratio			

**Table 3-6 Equivalent Properties for Tubesheet for Model 51F SG (Surry)**

Temperature (°F)	Out-of-Plane		In-Plane	
	E (Msi)	G (Msi)	E (Msi)	G (Msi)
70				
200				
300				
400				
500				
600				
700				

a,c,c

**Table 3-7 Equivalent Properties for Tubesheet for Model 44F SG (Turkey Point)**

Temperature (°F)	Out-of-Plane		In-Plane	
	E (Msi)	G (Msi)	E (Msi)	G (Msi)
70				
200				
300				
400				
500				
600				
700				

a,c,c



**Figure 3-1 Typical Representation of Severed Divider Plate Condition; Model 51F**



**Figure 3-2 Typical Solid Model for Intact Divider Plate; Model 44F**  
(Turkey Point Units 3 & 4 configuration shown)



**Figure 3-3 3-D FEA Mesh, View Down Z-axis**  
(51F configuration shown)



**Figure 3-4 3-D FEA Mesh, View Down Y-Axis**  
(51F configuration shown)

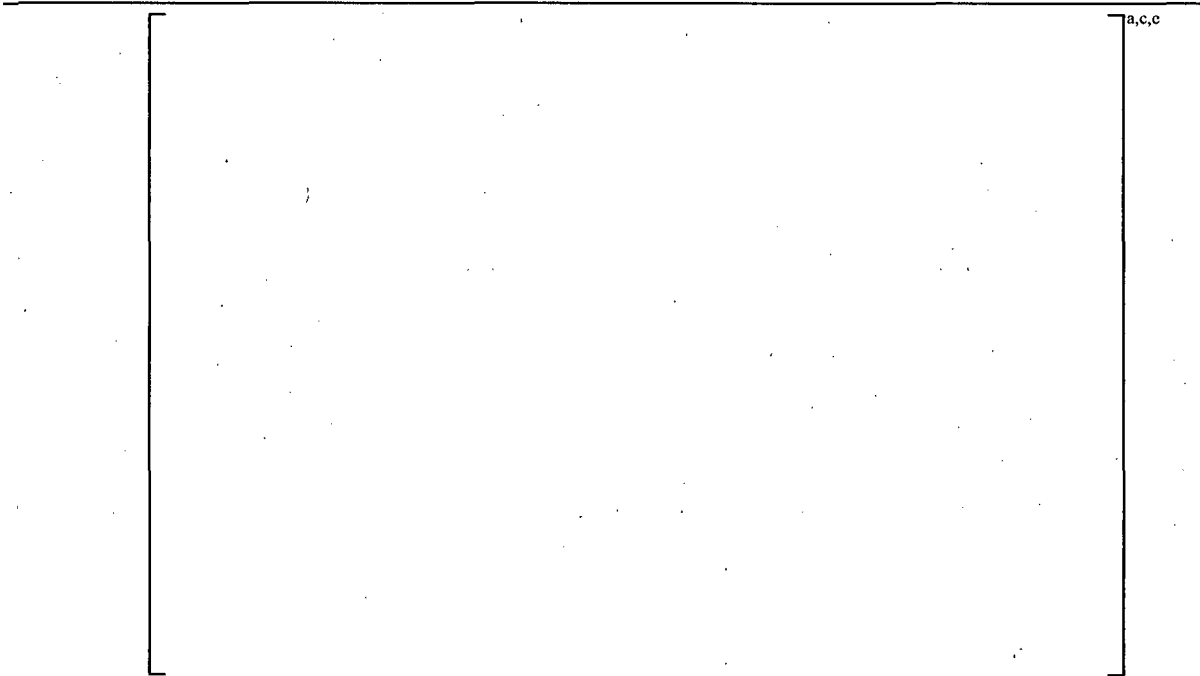


**Figure 3-5 3-D FEA Mesh, View Down X-Axis**  
(51F configuration shown)



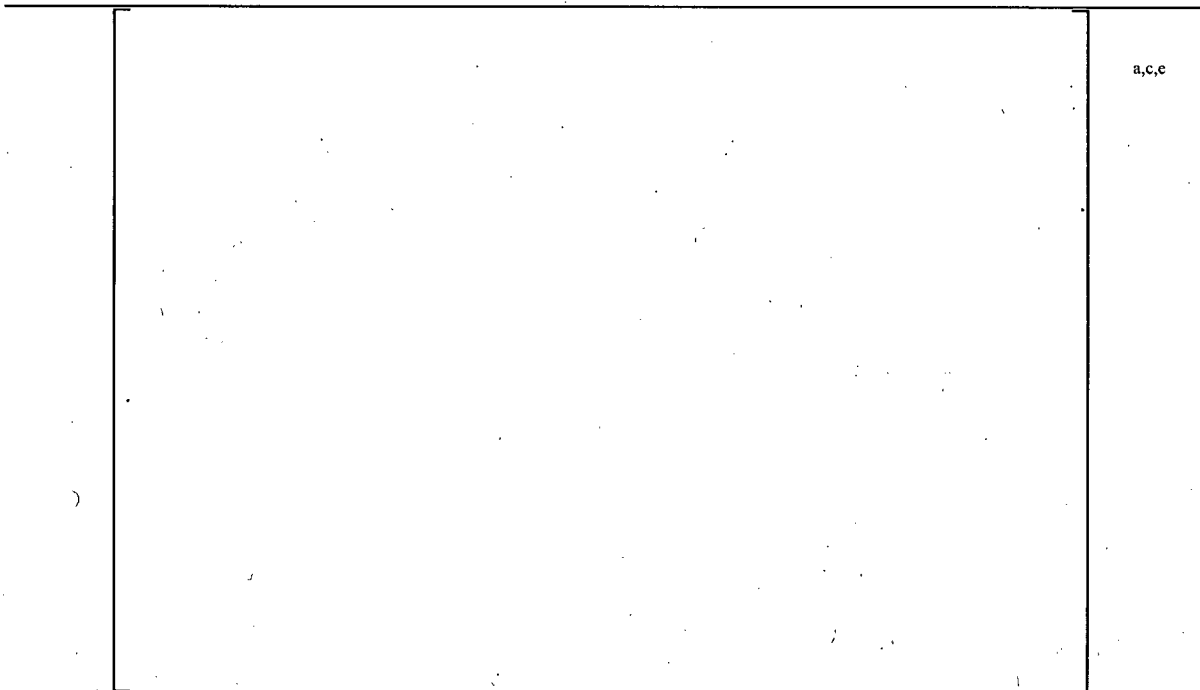
**Figure 3-6 3-D FEA Results of NOP Thermal Analysis**  
(51F configuration shown)



**Figure 3-7 3-D FEA Results of Thermal-Structural Analysis, Y Deformation**  
(51F configuration shown)



**Figure 3-8 3-D FEA Results of Thermal-Structural Analysis, X Deformation on Hot Leg Face**  
(51F configuration shown)



a,c,e

**Figure 3-9 3-D FEA Results of Thermal-Structural Analysis, Z Deformation on Hot Leg  
(51F configuration shown)**

a,c,e



**Figure 3-10 3-D FEA Results of SLB Thermal Analysis  
(51F configuration shown)**



**Figure 3-11 3-D FEA Results of SLB Thermal-Structural Analysis, X Deformation on Hot Leg Face  
(51F configuration shown)**



**Figure 3-12 3-D FEA Results of SLB Thermal-Structural Analysis, Z Deformation on Hot Leg Face  
(51F configuration shown)**

### 3.3 CALCULATION OF MEAN H\* FROM C<sup>2</sup> MODEL

#### 3.3.1 Method Discussion

The structural finite element analysis is based on a 2-D pseudo sub-model of the SG tubesheet and corresponding tube throughout the entire tubesheet thickness of approximately 21 inches. This model is then quartered to simplify the computations as seen in Figure 3-13.

Each tubesheet radius of each SG model is computed and graphed separately. At each tubesheet radius, there are nine elevations at which the contact pressure is calculated. For each operating condition, a thermal and thermal-structural analysis was performed with the 3-D FEA model (see Sections 3.1 and 3.2) to determine the tubesheet displacements used as input to the square cell model to calculate the contact pressures of the tubes with regards to the tubesheet. All of the analyses were static and linear elastic.



Figure 3-13 Sub-Model for Computational Analysis

#### 3.3.2 Development of Displacements for Square Cell

The displacements to apply to the square cell model are calculated from the displacements on the 3-D model using a finite difference technique to approximate the strain. The applied displacements simulate the strain across one-half of one pitch of the steam generator from all of the loads applied to the 3-D FEA model. There are two displacements to consider, those in the X-direction and those in the Z-direction (both in the same plane). For calculation of the displacements in the X-direction, the X-displacements on the hot leg face of the perforated section of the tubesheet are utilized. After being exported from ANSYS, they are processed using a finite difference method to calculate the strain, which is the derivative of displacement. This utilizes the central difference formula of second order (Reference 3-5, pp 83-85):

$$\varepsilon_i = \frac{\partial U_{x,i}}{\partial x} \approx \frac{U_{x,i+1} - U_{x,i-1}}{2\Delta x} \quad (\text{Equation 3-1})$$

At the edges of the perforated region, of necessity, the forward and backward differences of second order are used:

$$\begin{aligned}\varepsilon_i &= \frac{\partial U_{x,i}}{\partial x} \approx \frac{-U_{x,i+2} + 4U_{x,i+1} - 3U_{x,i}}{2\Delta x} \\ \varepsilon_i &= \frac{\partial U_{x,i}}{\partial x} \approx \frac{+U_{x,i-2} - 4U_{x,i-1} + 3U_{x,i}}{2\Delta x}\end{aligned}\quad (\text{Equation 3-2})$$

The displacement to apply to the square cell model is the strain times the length of the model, which is one-half of a pitch:

$$\Delta x_{\text{squarecell}} = 0.5 * P * \varepsilon_x \quad (\text{Equation 3-3})$$

The calculation of the Z-displacements uses the Z-displacements from the 3-D FEA model which are two pitches back from the hot leg face. A similar central difference formula is used to calculate the derivative:

$$\varepsilon_i = \frac{\partial U_{z,i}}{\partial z} \approx \frac{U_{z,i+2} - U_{z,i}}{2\Delta z} \quad (\text{Equation 3-4})$$

This equation is slightly modified to calculate the strain in the Z-direction one pitch back from the cut face of the 3-D model. This is necessary because the cut face has a symmetry condition in the Z-direction; therefore, the strain in the Z-direction necessarily vanishes there. Since the displacement is zero on that face, the equation can be simplified:

$$\varepsilon_i = \frac{\partial U_{z,i}}{\partial z} \approx \frac{U_{z,i+2}}{2P} \quad (\text{Equation 3-5})$$

Calculation of the applied displacements from the strain is identical:

$$\Delta z_{\text{squarecell}} = 0.5 * P * \varepsilon_z \quad (\text{Equation 3-6})$$

### 3.3.3 Discussion of Significant Assumptions

The axial thermal profile for the tubesheet is discussed in Section 3.2. In the thermal analysis, the secondary side of the tubesheet was assumed to be at a temperature equal to the average of the steam temperature and the feedwater temperature.

The dimensions used for the finite element model were consistent with the current licensing basis.

The divider plate was assumed to have the top five inches removed to account for a potentially degraded tubesheet to divider plate weld as discussed in Section 3.2.

The current results exclude any residual contact pressure effects from the tube hydraulic expansion.

---

For the connections between the tube and tubesheet, this model uses a friction coefficient of [ ]<sup>a,c,e</sup> (Reference 3-2), and a pinball radius of [ ]<sup>a,c,e</sup> inches, which is half the value of the surface roughness from Reference 3-15. The pinball radius is the tolerance within which contact at a node is assumed by the structural code. The analysis also uses a normal stiffness factor of [ ]<sup>a,c,e</sup>, which dictates how quickly the model will converge depending on the degree of bending deformation, which was based on several trials that defined this value for acceptable convergence of the model.

Concerning the tube bending in the tubesheet, the square cell model does not use the Goodier model to assume the tubesheet collar is a continuous structure. The applied loading on the tubesheet bends the tube. This bending is caused by temperature change as well as the pressure differential across the tubesheet and increases contact pressure. Neglecting tubesheet bending is conservative because the increased contact pressure between the tube and the tubesheet would reduce the H\* distance.

### 3.3.4 Input

The input for this analysis consists of steam generator dimensions for the plants to be analyzed, material properties from the ASME code, and pressure and temperature conditions from the PCWG parameters and transients. The dimensions, the material properties, the PCWG parameters used for the 44F and 51F models, the input for the Model 44Fs, the input for the Model 51Fs are taken from Reference 3-1 and 3-2.

Because the analysis is a static, linear, elastic methodology, the material properties used as inputs are the elastic moduli and coefficients of thermal expansion. The tubesheet is SA-508 Class 2A and the tube is Alloy 600 Thermally Treated (TT). The modulus of elasticity and coefficients of thermal expansion are the same as in the current licensing bases, References 3-1 and 3-2.

### 3.3.5 Geometry

Figure 3-14 shows a representation of the solid model used. The model was created in ANSYS Workbench Design Modeler. The associated representative dimensions for all models are shown in Figure 3-15.

### 3.3.6 Mesh

The mesh used in the analysis combines the tube and tubesheet in one model and creates one mesh for both pieces. This grid of nodes allows for easy post-processing and interpolation of deformations on the face. The density in this region is judged to be adequate from experience and comparison to prior models (i.e., Reference 3-6). The actual mesh for all models analyzed is shown in Figure 3-16.



**Figure 3-14 Representative Solid Model**



**Figure 3-15 Representative Dimensions for All Models**



a,c,e

**Figure 3-16 Implemented Model Mesh, View Down Z-Axis**

### 3.3.7 Boundary Conditions

The applied boundary conditions consisted of pressure loads, thermal loads, and constraints. The pressure loads consisted of the crevice pressure and the pressure difference inside the tube. The thermal loads were applied as fixed temperature boundary conditions on the bodies for the thermal analysis. Three constraints applied.

1. The upper edge of the model was constrained in the X-direction,
2. The lower edge of the model was constrained in the Y-direction.
3. The pressure differential on the tube was determined as the difference between the primary pressure on the tube ID and the crevice pressure on the tube OD.

The application of these boundary conditions is shown in Figure 3-17.

All of the applied loads and temperatures are described in Section 3.2.

(Note: For analytical convenience, the coordinate system for this model is X-Y, which is equivalent to the X-Z SG coordinates as noted in Section 2.)



**Figure 3-17 Boundary Conditions for All Models**

---

### 3.3.8 C<sup>2</sup> FEA Results

Inputs and contact pressure plots of the finite element analysis (FEA) results for each individual model, radius and elevation are included in this section. The thermal analysis results are steady-state with fixed boundary conditions (Reference 3-8).

Within each table, the explanations of the categories are as follows: TS Elevation stands for tubesheet elevation,  $\Delta X$  and  $\Delta Z$  represent the displacement in the respective direction of the square cell model, delta P represents the difference between the reference pressure and the crevice pressure which was empirically determined, temperature is self explanatory, and  $P_{con}$  Theta represents the contact pressure between the tube and tubesheet.

### 3.3.9 Model 44F (Turkey Point 3 & 4) FEA Results

The tabular results of the Model 44F FEA analysis are in Tables 3-8 through 3-13. These results are used to produce the graphical results for each tubesheet radius in Figures 3-18 to 3-23. Tables are provided for NOP and SLB conditions at each tubesheet radius.

### 3.3.10 Model 51F (Surry 1 & 2) FEA Results

The tabular results of the Model 51F FEA analysis are in Tables 3-14 through 3-19. These results are used to produce the graphical results for each radius in Figures 3-24 to 3-29. Tables are provided for the NOP and SLB conditions at each tubesheet radius.

### 3.3.11 Model 44F Contact Pressure Profiles

The results of the FEA analysis for the Model 44F that were calculated in Section 3.3.9 are shown below in Figure 3-18 through 3-23. These figures show the contact pressure trends between the normal operating condition versus the steam line break conditions at various elevations between 0.0 and 21.810 inches, where 0.0 represents the top of the tubesheet and 21.810 represents the bottom of the tubesheet.

### 3.3.12 Model 51F Contact Pressure Profiles

The results of the FEA analysis for the Model 51F that were calculated in Section 3.3.10 are shown below in Figures 3-24 through 3-29. These figures show the contact pressure trends between the normal operating condition versus the steam line break conditions at various elevations between 0.0 and 21.030 inches, where 0.0 represents the top of the tubesheet and 21.030 represents the bottom of the tubesheet.

Table 3-8 Model 44F Turkey Point 3 &amp; 4 Inputs and Results, 2.655 in Radius

NOP						
	TS Elevation	$\Delta X$	$\Delta Z$	$\Delta P$	Temperature	$P_{con}$ Theta
	in	in	in	psi	°F	psi
BTS	0.000					
	2.000					
	3.523					
	5.442					
NA	10.905					
	16.368					
	18.287					
	19.810					
TTS	21.810					

a,c,e

SLB						
	TS Elevation	$\Delta X$	$\Delta Z$	$\Delta P$	Temperature	$P_{con}$ Theta
	in	in	in	psi	°F	psi
BTS	0.000					
	2.000					
	3.523					
	5.442					
NA	10.905					
	16.368					
	18.287					
	19.810					
TTS	21.810					

a,c,e

**Table 3-9 Model 44F Turkey Point 3 & 4 Inputs and Results, 7.291 in Radius**

NOP						
	TS Elevation	$\Delta X$	$\Delta Z$	$\Delta P$	Temperature	$P_{con}$ Theta
	in	in	in	psi	°F	psi
BTS	0.000					
	2.000					
	3.523					
	5.442					
NA	10.905					
	16.368					
	18.287					
	19.810					
TTS	21.810					

a,c,e

SLB						
	TS Elevation	$\Delta X$	$\Delta Z$	$\Delta P$	Temperature	$P_{con}$ Theta
	in	in	in	psi	°F	psi
BTS	0.000					
	2.000					
	3.523					
	5.442					
NA	10.905					
	16.368					
	18.287					
	19.810					
TTS	21.810					

a,c,e

**Table 3-10 Model 44F Turkey Point 3 & 4 Inputs and Results, 18.171 in Radius**

NOP							
	TS Elevation	$\Delta X$	$\Delta Z$	$\Delta P$	Temperature	$P_{con}$ Theta	
	in	in	in	psi	°F	psi	
BTS	0.000						a,c,e
	2.000						
	3.523						
	5.442						
NA	10.905						
	16.368						
	18.287						
	19.810						
TTS	21.810						

SLB							
	TS Elevation	$\Delta X$	$\Delta Z$	$\Delta P$	Temperature	$P_{con}$ Theta	
	in	in	in	psi	°F	psi	
BTS	0.000						a,c,e
	2.000						
	3.523						
	5.442						
NA	10.905						
	16.368						
	18.287						
	19.810						
TTS	21.810						

**Table 3-11 Model 44F Turkey Point 3 & 4 Inputs and Results, 28.210 in Radius**

NOP						
	TS Elevation	$\Delta X$	$\Delta Z$	$\Delta P$	Temperature	$P_{con}$ Theta
	in	in	in	psi	°F	psi
BTS	0.000					
	2.000					
	3.523					
	5.442					
NA	10.905					
	16.368					
	18.287					
	19.810					
TTS	21.810					

a,c,e

SLB						
	TS Elevation	$\Delta X$	$\Delta Z$	$\Delta P$	Temperature	$P_{con}$ Theta
	in	in	in	psi	°F	psi
BTS	0.000					
	2.000					
	3.523					
	5.442					
NA	10.905					
	16.368					
	18.287					
	19.810					
TTS	21.810					

a,c,e

**Table 3-12 Model 44F Turkey Point 3 & 4 Inputs and Results, 34,598 in Radius**

NOP						
	TS Elevation	$\Delta X$	$\Delta Z$	$\Delta P$	Temperature	$P_{con}$ Theta
	in	in	in	psi	°F	psi
BTS	0.000					
	2.000					
	3.523					
	5.442					
NA	10.905					
	16.368					
	18.287					
	19.810					
TTS	21.810					

a,c,e

SLB						
	TS Elevation	$\Delta X$	$\Delta Z$	$\Delta P$	Temperature	$P_{con}$ Theta
	in	in	in	psi	°F	psi
BTS	0.000					
	2.000					
	3.523					
	5.442					
NA	10.905					
	16.368					
	18.287					
	19.810					
TTS	21.810					

a,c,e

**Table 3-13 Model 44F Turkey Point 3 & 4 Inputs and Results, 48.288 in Radius**

NOP						
	TS Elevation	$\Delta X$	$\Delta Z$	$\Delta P$	Temperature	$P_{con}$ Theta
	in	in	in	psi	°F	psi
BTS	0.000					
	2.000					
	3.523					
	5.442					
NA	10.905					
	16.368					
	18.287					
	19.810					
TTS	21.810					

a,c,e

SLB						
	TS Elevation	$\Delta X$	$\Delta Z$	$\Delta P$	Temperature	$P_{con}$ Theta
	in	in	in	psi	°F	psi
BTS	0.000					
	2.000					
	3.523					
	5.442					
NA	10.905					
	16.368					
	18.287					
	19.810					
TTS	21.810					

a,c,e

**Table 3-14 Model 51F Surry 1 & 2 Inputs and Results, 4.016 in Radius**

NOP							
	TS Elevation	$\Delta X$	$\Delta Z$	$\Delta P$	Temperature	$P_{con}$ Theta	
	in	in	in	psi	°F	psi	
BTS	0.000						a,c,e
	2.000						
	4.000						
	6.000						
NA	10.515						
	16.901						
	19.030						
	20.030						
TTS	21.030						

SLB							
	TS Elevation	$\Delta X$	$\Delta Z$	$\Delta P$	Temperature	$P_{con}$ Theta	
	in	in	in	psi	°F	psi	
BTS	0.000						a,c,e
	2.000						
	4.000						
	6.000						
NA	10.515						
	16.901						
	19.030						
	20.030						
TTS	21.030						

**Table 3-15 Model 51F Surry 1 & 2 Inputs and Results, 11.722 in Radius**

NOP							
	TS Elevation	$\Delta X$	$\Delta Z$	$\Delta P$	Temperature	$P_{con}$ Theta	
	in	in	in	psi	°F	psi	
BTS	0.000						a,c,e
	2.000						
	4.000						
	6.000						
NA	10.515						
	16.901						
	19.030						
	20.030						
TTS	21.030						

SLB							
	TS Elevation	$\Delta X$	$\Delta Z$	$\Delta P$	Temperature	$P_{con}$ Theta	
	in	in	in	psi	°F	psi	
BTS	0.000						a,c,e
	2.000						
	4.000						
	6.000						
NA	10.515						
	16.901						
	19.030						
	20.030						
TTS	21.030						

**Table 3-16 Model 51F Surry 1 & 2 Inputs and Results, 20.498 in Radius**

NOP							
	TS Elevation	$\Delta X$	$\Delta Z$	$\Delta P$	Temperature	P <sub>con</sub> Theta	
	in	in	in	psi	°F	psi	
BTS	0.000						a,c,e
	2.000						
	4.000						
	6.000						
NA	10.515						
	16.901						
	19.030						
	20.030						
TTS	21.030						

SLB							
	TS Elevation	$\Delta X$	$\Delta Z$	$\Delta P$	Temperature	P <sub>con</sub> Theta	
	in	in	in	psi	°F	psi	
BTS	0.000						a,c,e
	2.000						
	4.000						
	6.000						
NA	10.515						
	16.901						
	19.030						
	20.030						
TTS	21.030						

**Table 3-17 Model 51F Surry 1 & 2 Inputs and Results, 30.193 in Radius**

NOP						
	TS Elevation	$\Delta X$	$\Delta Z$	$\Delta P$	Temperature	P <sub>con</sub> Theta
	in	in	in	psi	°F	psi
BTS	0.000					
	2.000					
	4.000					
	6.000					
NA	10.515					
	16.901					
	19.030					
	20.030					
TTS	21.030					

a,c,e

SLB						
	TS Elevation	$\Delta X$	$\Delta Z$	$\Delta P$	Temperature	P <sub>con</sub> Theta
	in	in	in	psi	°F	psi
BTS	0.000					
	2.000					
	4.000					
	6.000					
NA	10.515					
	16.901					
	19.030					
	20.030					
TTS	21.030					

a,c,e

**Table 3-18 Model 51F Surry 1 & 2 Inputs and Results, 48.613 in Radius**

NOP							
	TS Elevation	$\Delta X$	$\Delta Z$	$\Delta P$	Temperature	$P_{con}$ Theta	
	in	in	in	psi	°F	psi	
BTS	0.000						a,c,e
	2.000						
	4.000						
	6.000						
NA	10.515						
	16.901						
	19.030						
	20.030						
TTS	21.030						

SLB							
	TS Elevation	$\Delta X$	$\Delta Z$	$\Delta P$	Temperature	$P_{con}$ Theta	
	in	in	in	psi	°F	psi	
BTS	0.000						a,c,e
	2.000						
	4.000						
	6.000						
NA	10.515						
	16.901						
	19.030						
	20.030						
TTS	21.030						

**Table 3-19 Model 51F Surry 1 & 2 Inputs and Results, 58.308 in Radius**

NOP						
	TS Elevation	$\Delta X$	$\Delta Z$	$\Delta P$	Temperature	$P_{con}$ Theta
	in	in	in	psi	°F	psi
BTS	0.000					
	2.000					
	4.000					
	6.000					
NA	10.515					
	16.901					
	19.030					
	20.030					
TTS	21.030					

a,c,e

SLB						
	TS Elevation	$\Delta X$	$\Delta Z$	$\Delta P$	Temperature	$P_{con}$ Theta
	in	in	in	psi	°F	psi
BTS	0.000					
	2.000					
	4.000					
	6.000					
NA	10.515					
	16.901					
	19.030					
	20.030					
TTS	21.030					

a,c,e



**Figure 3-18 Model 44F Contact Pressure Results, 2.655 in Radius**



**Figure 3-19 Model 44F Contact Pressure Results, 7.219 in Radius**

0-TS Elevation is the Top of the Tubesheet



**Figure 3-20 Model 44F Contact Pressure Results, 18.171 in Radius**



**Figure 3-21 Model 44F Contact Pressure Results, 28.210 in Radius**

0-TS Elevation is the Top of the Tubesheet



**Figure 3-22 Model 44F Contact Pressure Results, 34.598 in Radius**



**Figure 3-23 Model 44F Contact Pressure Results, 48.288 in Radius**

0-TS Elevation is the Top of the Tubesheet



**Figure 3-24 Model 51F Contact Pressure Results, 4.016 in Radius**



**Figure 3-25 Model 51F Contact Pressure Results, 11.722 in Radius**

0-TS Elevation is the Top of the Tubesheet



**Figure 3-26 Model 51F Contact Pressure Results, 20.498 in Radius**



**Figure 3-27 Model 51F Contact Pressure Results, 30.193 in Radius**

0-TS Elevation is the Top of the Tubesheet



a,c,e

**Figure 3-28 Model 51F Contact Pressure Results, 48.613 in Radius**



a,c,e

**Figure 3-29 Model 51F Contact Pressure Results, 58.308 in Radius**

0-TS Elevation is the Top of the Tubesheet

### 3.3.13 Mean H\* Calculations

Once the contact pressures were calculated for each radius of each model, it is then possible to calculate a mean H\* for each radius of each model. The equation used is the same as in Reference 3-1 and 3-2, Equation 1-3. Table 3-20 contains the inputs used to determine the H\*'s along with the contact pressures.

Equation 1-3 from References 3-1 and 3-2 generates the accumulated pull out load throughout the thickness of the tubesheet at each elevation. These accumulated pull out loads are then integrated using the trapezoidal rule along with the predetermined pull out loads for each model (References 3-1 and 3-2) to generate the mean H\* for that radius. Table 3-21 shows the results of these calculations for each radius of each mode. From these values, the critical radius is determined by the largest value for each model.

**Table 3-20 H\* Input Summary**  
(References 3-1 and 3-2)

	NOP	SLB
SG Model/Tube OD	End cap Load (lb)	End cap Load (lb)
44F/[ ] <sup>a,c,e</sup>	[ ] <sup>a,c,e</sup>	[ ] <sup>a,c,e</sup>
51F/[ ] <sup>a,c,e</sup>	[ ] <sup>a,c,e</sup>	[ ] <sup>a,c,e</sup>

**Table 3-21 Summary of H\* Mean Values**  
(all dimensions in inches)

SG Model	Radius	NOP H* <sup>(1)</sup>
44F	2.655	[ ] <sup>a,c,e</sup>
	7.219	[ ]
	18.171	[ ]
	28.21	[ ]
	34.598	[ ]
	48.288	[ ]
51F	4.016	[ ]
	11.772	[ ]
	20.498	[ ]
	30.193	[ ]
	48.613	[ ]
	58.308	[ ]

(1)The limiting condition for both the Model 44F and Model 51F is the normal operating condition.

---

### 3.4 CALCULATION OF PROBABILISTIC H\* USING THE C2 MODEL

This section provides a comparison between the square cell ( $C^2$ ) structural model and the licensing basis structural model in terms of the probabilistic evaluation of  $H^*$ . The Monte-Carlo simulation process by which the distribution of  $H^*$  is computed for a given CTE response surface is described in Reference 3-14. The analyses described in this section investigate the relative behavior of the square cell and licensing basis models in the local region of CTE space (tube-CTE, tubesheet-CTE) determined in the current licensing basis to include the 95<sup>th</sup> percentile value of  $H^*$ . Guidance for the methods discussed in this section was taken from Reference 3-10.

The square cell ( $C^2$ ) analysis is an independent method of modeling the contact pressure distribution between the tube and the tubesheet used to calculate  $H^*$ . The results can be compared to those of the licensing basis for the permanent  $H^*$  ARC. The results of using the square cell analysis show that the mean value of  $H^*$  and the probabilistic estimate of the  $H^*$  value at the required probability level change compared to the existing licensing basis values. The Model 51F SG probabilistic  $H^*$  value increases by 2.16 inches and the Model 44F SG probabilistic value increases by 2.71 inches. These changes to the current licensing basis values are caused by the calculation of updated tubesheet displacements and contact pressures than were documented in References 3-1 and 3-2 and discussed above in Sections 3.2 and 3.3 of this report.

#### 3.4.1 Assumptions

The assumptions made for the structural analyses of the tubes and tubesheet also apply to the analysis of the probabilistic value of  $H^*$ . Sections 3.1 through 3.3 of this report provide a detailed description of those assumptions. Additional assumptions and observations that apply only to the probabilistic  $H^*$  and Monte Carlo (MC) analysis are:

1. The critical region of the  $H^*$  response surface will remain at a combination of decreasing tube CTE ( $-n\sigma_T$ ) and increasing tubesheet CTE ( $+n\sigma_T$ ). This assumption was previously shown to maximize the value of  $H^*$ . At large variations from the mean, the tubesheet will grow away from the tube and there will be zero contact pressure contribution from thermal effects ("lock-up"). Variations of Young's modulus has been shown to have negligible effect on  $H^*$  in prior analyses.
2. Both the  $C^2$  model and the thick shell model represent the similar physical structure; thus, both models are expected to yield the same trend in their response to variations of material properties.
3. In the range of interest (e.g., above the 90<sup>th</sup> percentile), the  $H^*$  rank order statistic results from a series of material property combinations, predicted by a full bundle Monte Carlo simulation with 10,000 trials, will remain essentially linear regardless of which structural model is applied. This assumption is shown to be true in the subsequent analysis.
4. The sensitivity of the square cell model contact pressure results to adjusting the tube length based on the crevice pressure distribution is similar to the curves developed for the  $H^*$  analysis in References 3-1 and 3-2. The crevice pressure adjustment curves from References 3-1 and 3-2 are reproduced in Figures 3-30 and Figure 3-31.

### 3.4.2 Methods Discussion

The process for the probabilistic analysis based on the  $C^2$  model is summarized in the following steps:

1. The structural response surface is determined in the current licensing basis, i.e., Figure 8-5 in the respective WCAP reports, References 3-1 and 3-2.
2. Based on the Monte Carlo evaluation using the specific response surfaces as documented in Reference 3-13, the values of the significant variables, the coefficients of thermal expansion of the tube and the tubesheet materials that lead to the required probabilistic values of  $H^*$  (i.e., 95 percent probability at 50 percent confidence), can be determined.
3. Application of the combination of coefficients of thermal expansion determined in Step 2 to the  $C^2$  model will yield the probabilistic values of  $H^*$  based on the  $C^2$  model. Because the inputs for the  $C^2$  model are taken from the output of the 3-D FEA model, this involves also performing 3-D FEA model analyses using the tubesheet CTE values.

The method for developing the comparison response surface using the square cell analysis begins with the Monte Carlo analysis results from the licensing basis analysis. The results for the upper 10 percent tail of the  $H^*$  distribution (e.g., rank order 9000 to rank order 10,000 in 10,000 simulations) from the licensing basis analysis were output as a 4 column by 1000 row vector. The values in the vector correspond to the rank order statistic, the  $H^*$  value at a given rank order, the variation in the tubesheet CTE about its mean value in terms of  $n\sigma$ , and the variation in the tube CTE about its mean value in terms of  $n\sigma$  where  $n\sigma$  is the number and direction (positive or negative) of standard deviations added to the mean value of the respective CTEs (see for example Table 3-25). The mean values of CTEs for the tube and the tubesheet and their respective standard deviations ( $[ \quad ]^{a,c,c}$  percent for the tube material CTE and  $[ \quad ]^{a,c,c}$  percent for the tubesheet material) are taken from the licensing basis documentation, References 3-1 and 3-2.

The  $H^*$  results from the licensing basis analysis include the effect of the tubesheet thermal distribution offset, and a 0.3 inch adder to address potential uncertainty in the location of the bottom of the expansion transition (BET) at the top of the tubesheet (TTS) but do not include the adjustment for crevice pressure or any benefit from the installation process (e.g., residual contact pressure). Section 6.4.5, Section 6.4.8, and Section 8.1.1 in Reference 3-1 discuss the effects of crevice pressure and the reasons for adjusting the final tube length in the  $H^*$  calculation process. Figures 3-30 and 3-31 reproduce the applicable crevice pressure adjustment curves from References 3-1 and 3-2 for the Model 44F and Model 51F SGs, respectively.

The results of the licensing basis analysis were considered as a function of the combined uncertainties of the tube and tubesheet CTE vs.  $H^*$ . It is possible to use the combined uncertainty approach because the limiting  $H^*$  result occurs at a combination of tube and tubesheet properties with increasing (positive) tubesheet CTE variations and decreasing (negative) tube CTE variations. Because the combination of the tube and the tubesheet properties that lead to the maximum value of  $H^*$  always occur in the same

quadrant, the sign of the material property variation is conserved and the region of the response surface to be compared is also conserved.

Reference 3-13 discusses the method for combining the significant variables for probabilistic analysis. Figure 3-32 shows the relation between the combined significant variables and the  $H^*$  values above the 90<sup>th</sup> percentile from the licensing basis analysis for a typical SG candidate for  $H^*$ . The same general form of the data occurs in each of the models of SG considered when evaluated in this fashion. The lower bound of the data is termed the "break line." The break line is the maximum value of  $H^*$  for a constant value of the combined significant variables affecting  $H^*$ . Therefore, the break line contains the limiting  $H^*$  for the specific SG model being considered. The "break line" can be fit by proper selection of the data points that define the lower bound of the data. Because the value of the combined significant variables are taken directly from the rank ordered results from the original analysis, the break line can also be defined in terms of the rank order instead of  $H^*$  values. Figure 3-33 shows the break line defined by the rank order of the points selected.

The break line is used to determine specific values of the tube and tubesheet CTE to be used in a series of structural analysis cases using both the 3-D FEA model and the  $C^2$  model. Note that the specific values of tubesheet CTE are always greater than the mean and the specific values of tube CTE are always less than the mean. The points selected are typically above and below the required probabilistic estimates (rank order) to produce a conservative result that bounds the needed value of  $H^*$  without extrapolating data. The probabilistic estimates (defined as the rank order from 10,000 simulations) required for each of the limiting plants in the  $H^*$  fleet are listed in Table 3-22. The points selected for each of the limiting plants in the  $H^*$  fleet are listed in Table 3-23.

The selected values of the tubesheet CTE are used in a 3-D finite element analysis of the lower SG complex. The models, analysis method, assumptions and inputs to the lower SG complex analysis are the same to those described in References 3-1 and 3-2 but the model is modified to eliminate the upper five inches of the divider plate and re-meshed to provide the proper output displacement for the  $C^2$  model. The resulting tubesheet displacements calculated from the model using the increased tubesheet CTE, with the matching decreased tube CTE properties, become inputs to the square cell model analysis as described in Section 2 of this report. The resulting contact pressures are then used to calculate the value of  $H^*$  for that combination of tube and tubesheet CTE. This process is repeated for each of the selected data points along the break line. The  $H^*$  values calculated using the new inputs to the square cell model correspond to the rank order statistic from the licensing basis.

The  $H^*$  values for the same values of rank order statistic in the licensing basis and the square cell analysis are directly compared by plotting the resulting  $H^*$  values as a function of the rank order statistic. See Figure 3-34 for the typical result based on the NOP condition analysis. The data in Figure 3-34 can be used to develop a relationship to interpolate the  $H^*$  value of the rank order statistic based on the required estimate given in Table 3-22. The final  $H^*$  value for the desired rank order statistic is the  $H^*$  value obtained from the interpolation of the bounding  $H^*$  values plus the crevice pressure adjustment. Figure 8-1 in References 3-1 and 3-2 shows the crevice pressure distribution adjustment curves for the Model 44F and Model 51F SGs, respectively.

The order statistic for higher confidence intervals (e.g., 95 percent) is calculated using a method described in Reference 3-14. This method involves calculating the difference in rank order between the

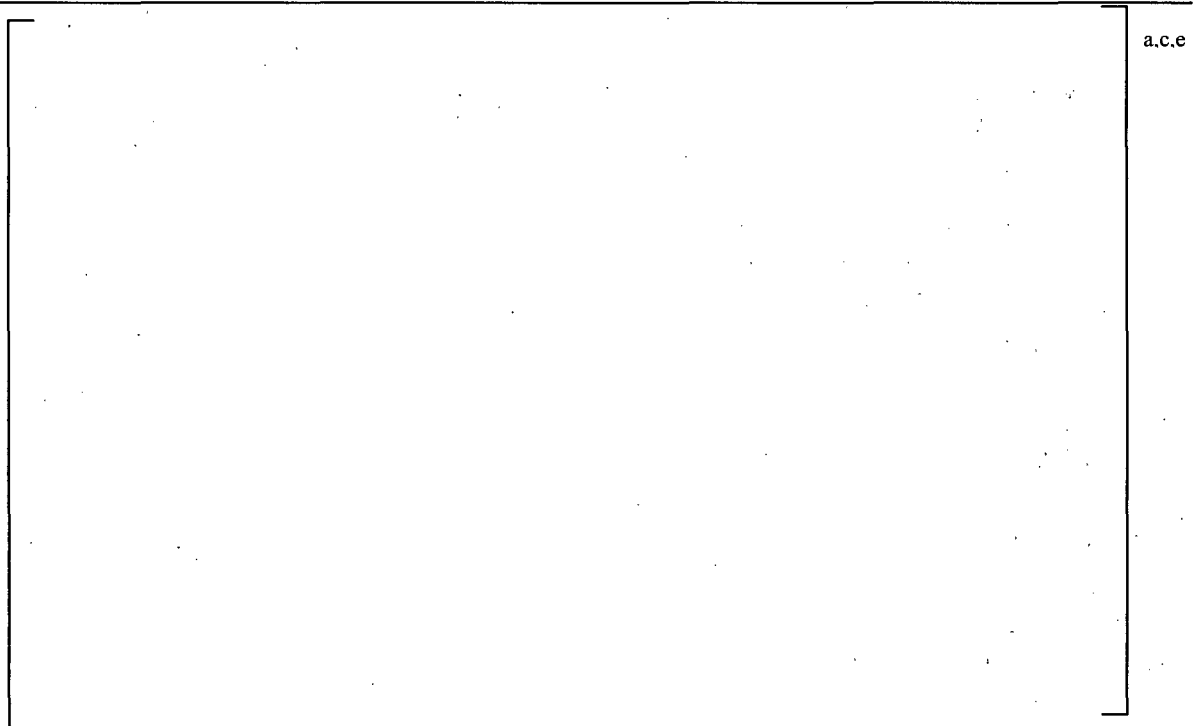
---

95/50 probability and confidence estimate and the next highest probabilistic estimate value (e.g., 96 percent) using standard equations and error functions from Reference 3-14. The final  $H^*$  value for the desired rank order statistic is the  $H^*$  value obtained from the interpolation of the bounding  $H^*$  values plus the crevice pressure adjustment.

The difference in the required order statistic for the whole bundle  $H^*$  estimates and the whole plant  $H^*$  estimates (see Table 3-22) is based on the population of the tubes in the plant. The number of tubes in a plant depends on the SG model and the number of SGs in a plant. For simplicity, the entire design population of tubes, including currently plugged tubes, is considered. The difference between a whole bundle value of 9500 (95/50) and a whole plant value is defined by the 9500th  $H^*$  value for the combined results of 10,000 simulations of each SG in the plant. For example, consider a 4-loop plant: Performing the 10,000 trial Monte Carlo simulation four times to represent four different generators yields four different sets of rank order vectors in terms of  $H^*$ , TS CTE variation and T CTE variation. All four vectors will be similar, but yield slightly different  $H^*$  values at the same rank order.

The value of the whole plant  $H^*$  is determined by first calculating four vectors of  $H^*$  values corresponding to four steam generators. A fifth vector is then produced whose  $i^{\text{th}}$  element consists of the maximum  $H^*$  among the  $i^{\text{th}}$  elements of the four beginning vectors. This vector is then sorted, and the rank order statistic for 95/50 is the 9500th value. This value of  $H^*$  is then searched for in an ordered input vector to determine approximately what rank order statistic for a single steam generator corresponds to the 9500th rank order  $H^*$  for an entire plant.

To apply the method discussed herein, it is necessary to identify the whole bundle rank order of the  $H^*$  value that is the same as the 95 percent  $H^*$  value for the whole plant. For example, the value of the 95 percent  $H^*$  for the four SGs in a Model F plant is equivalent to the [ ]<sup>a,c,c</sup>  $H^*$  value for a single Model F bundle. Other models of SGs have different tube populations than the Model F; therefore, the equivalent rank order for the different model SG will also be different. The difference between the whole bundle  $H^*$  value and the whole plant  $H^*$  value comes from using the tube and tubesheet CTE values associated with the  $H^*$  value for the whole plant 95 percent in the calculations using the  $C^2$  model.



a.c.e

**Figure 3-30: Model 44F Crevice Pressure Adjustment Curve**  
(from Reference 3-1)



a.c.e

**Figure 3-31: Model 51F Crevice Pressure Adjustment Curve**  
(from Reference 3-2)

---

### 3.4.3 Input

The necessary inputs for the probabilistic analysis using the  $C^2$  model are:

- The limiting radius for  $H^*$  for the model SG of interest. The limiting tubesheet radius is the radial position on the tubesheet where the longest  $H^*$  distance occurs at the limiting operating condition at mean material properties.
- The limiting operating condition for  $H^*$  (NOP or SLB).
- The significant material properties, CTE for the tubesheet and tube material.

Table 3-24 specifies the limiting radius for  $H^*$  for the Model 44F and Model 51F SGs. The limiting radii for the different models of SG were determined using the  $C^2$  model and mean material properties as was done with the thick shell model in the licensing basis analysis. The limiting tubesheet radius was determined to be the same as in the current licensing basis for both the Model 51F and Model 44F SGs. Table 3-24 also specifies the limiting operating conditions for the Model 44F and Model 51F SGs.

The limiting operating condition for  $H^*$  is the operating condition that produces the most conservative (i.e., longest) predicted  $H^*$  depth. The operating conditions considered are normal operating condition at low temperature (average conditions), NOP or  $NOP_{LOW\ TAVG}$ , and main steam line break, SLB, consistent with the current licensing basis.

Typical upper 90<sup>th</sup> percentile Monte Carlo results are shown in Table 3-25, with the result of the combined value of the tube and tubesheet CTE in the fifth column of the table. The Monte Carlo results cover one thousand rank values (from the 90th percentile to the 100th percentile of 10,000 simulations) based on the Monte Carlo sampling performed in the current licensing basis. The values used in the analysis, and the exact rank order statistics required for the comparison of the  $H^*$  values generated by the square cell analysis to the  $H^*$  values in the existing licensing basis are given in Table 3-22 and Table 3-23. The typical range of values for the combined variable for all steam generators is between three and six.

The data in Table 3-23 were selected based on examining the reduced response surface from the existing licensing basis. The reduced response data for the Model 44F and Model 51F SGs are shown in Figures 3-35, 3-36, 3-38, and Figure 3-39. The bounding data in the reduced set from each of the reduced response data plots used to estimate the  $H^*$  values are listed in Table 3-25. The CTE variations for the tube and tubesheet materials used in the finite element analyses of the lower SG complex and the square cell analysis are given in Table 3-26 and Table 3-27.

The result of using the material properties in Table 3-26 in the finite element analysis of the lower SG complex is the tubesheet displacement as a function of elevation. This result, along with the variation in the tube properties described in Table 3-27 is used as input to the square cell analysis. The output from the square cell analysis is the contact pressure distribution between the tube and the tubesheet as a function of elevation. This contact pressure distribution is used to calculate the  $H^*$  values for the response surface comparison. A Poisson offset is also added to the final  $H^*$  values in order to account for the effect of including an end-cap load on the tube in the  $C^2$  analysis for  $H^*$  (see Section 3.5 for discussion). An end-cap load physically applied to the tube would act to reduce the outer diameter of the tube by reducing the

tube cross section. Application of the Poisson adjustment is conservative because of the counter-acting effect of Poisson expansion due to thermal axial expansion of the tube and bending of the tube portion within the tubesheet are ignored. The Poisson offset is added to the H\* result before the crevice pressure adjustment is determined because the Poisson adjustment is constant on the tube regardless of the final tube length as determined by the crevice pressure adjustment.

#### 3.4.4 Model 44F Results

The H\* values (without a crevice pressure adjustment) from the contact pressure distributions developed using the C<sup>2</sup> model at the limiting TS radius are shown in Table 3-28 together with the rank order of the input values as discussed above. The results shown in Table 3-28 are represented graphically in Figure 3-37.

The results shown in Table 3-28 are represented graphically in Figure 3-37. There is a difference in the existing licensing basis results for H\* at the given rank order statistics and the square cell model results. The H\* estimates based on the square cell model results are about two to three inches greater than those from the licensing basis. The linear fit between the H\* results for rank order [ ]<sup>a,c,e</sup> and [ ]<sup>a,c,e</sup> is very good, but there is a slight deviation from a perfect fit ( $R^2 < 1$ ) such that a slight decrease in slope occurs from rank order [ ]<sup>a,c,e</sup> to [ ]<sup>a,c,e</sup> if two separate linear fits are made of the data.

The linear fit used to interpolate the exact value of H\* at the desired rank order statistic for the Model 44F SG is given in Equation 3-7:

$$H^* \text{ Value} = [ ]^{a,c,e} \quad (\text{Equation 3-7})$$

The final values of H\*, with the corresponding crevice pressure length adjustment taken from Figure 3-30, are shown in Table 3-29.

#### 3.4.5 Model 51F Results

The contact pressure results from the Model 51F square cell analysis are based on the selected rank order statistics from the Model 51F Monte Carlo (MC) analysis. The resulting H\* values at the desired rank order statistics, without any crevice pressure adjustment, from the NOP contact pressure distributions at the limiting TS radius are shown in Table 3-30 for both the licensing basis method and application of the square cell model. The results shown in Table 3-30 are represented graphically in Figure 3-40.

The linear fit used to interpolate the value of H\* at the desired rank order statistic for the Model 51F SG is given in Equation 3-8:

$$H^* \text{ Value} = [ ]^{a,c,e} \quad (\text{Equation 3-8})$$

The final values of H\*, with the corresponding crevice pressure length adjustment taken from Figure 3-31 are shown in Table 3-31.



**Figure 3-32 Typical Result for Plotting the Combined Tube and Tubesheet CTE Values Against  $H^*$  from the Licensing Basis Analysis**



**Figure 3-33 Typical Result for Plotting the Combined Tube and Tubesheet CTE Values Against Monte Carlo Rank Order from the Licensing Basis Analysis**



**Figure 3-34 Typical Comparative H\* Curves from Selected Response Surface**



**Figure 3-35 Model 44F NOP Combined CTE<sub>T</sub> and CTE<sub>TS</sub> vs. Monte Carlo Rank Order**



**Figure 3-36 Reduced Model 44F NOP Response Data**



**Figure 3-37 Model 44F H\* Summary Showing Linear Fit Results**



**Figure 3-38 Model 51F SLB Combined T CTE and TS CTE as a Function of H\***



**Figure 3-39 Reduced Model 51F SLB Response Data**



**Figure 3-40 Model 51F H\* Summary Showing Linear Fit Results**

Table 3-22 Required Probabilistic Estimate for H\*

Model SG	Whole Bundle Estimate		Whole Plant Estimate		a,c,e
	95/50	95/95	95/50	95/95	
F					a,c,e
D5					
44F					
51F					
Notes:					
(1) Whole plant does not apply because SLB is limiting condition for H*					
(2) Values are the whole bundle rank orders based on whole plant rank order equivalent H* to recover the corresponding values of tube and tubesheet CTE.					

Table 3-23 Monte Carlo Data Used in Comparative Probabilistic Analysis

Model SG	Limiting Operating Condition	Rank Order Statistic (1)	Tubesheet CTE Variation (standard deviations)	Tube CTE Variation (standard deviations)	Alpha	a,c,e
F	NOP					
D5	SLB					
44F 3-Loop	NOP					
51F	NOP					
Notes: (1) Based on 10,000 simulations						



**Table 3-27 Negative Variations about the Mean Tube CTE used for FEA**

(Units of  $10^{-6}$  in/in/°F)

Temp. °F	Mean	Multiplier on Standard Deviation									
212	7.22										
300	7.40										
420	7.60										
500	7.70										
600	7.82										
628	7.85										

a,c,e

**Table 3-28 Bounding Model 44F H\* Results for Comparison Study**

(without  $P_{crev}$  Adjustment)

MC Rank in 10K Simulations	H* Result from Current Licensing Basis in.	H* Result from Square Cell Analysis in.

a,c,e

**Table 3-29 Summary of Model 44F Probabilistic Estimates**

Description	MC Rank in 10K Simulations	H*- C <sup>2</sup> (in.)	P <sub>crev</sub> (in.)	Poisson Offset (in.)	Final (in.)
Whole Bundle, 95/50					17.58
Whole Bundle, 95/95					17.62
Whole Plant, 95/50					17.79
Whole Plant, 95/95					17.80

a,c,e

**Table 3-30: Bounding Model 51F H\* Results for Comparison Study**

MC Rank in 10K Simulations	H* Result from Licensing Basis MC Study (in.)	H* Result from Square Cell Analysis (in.)
[ ]		] a.c.e
[ ]		] a.c.e
[ ]		] a.c.e

**Table 3-31: Summary of Model 51F Probabilistic Estimates**

Name	MC Rank #	H* - C <sup>2</sup> (in.)	Perev (in.)	Poisson Offset (in.)	Final (in.)
Whole Bundle, 95/50	[ ]			] a.c.e	17.41
Whole Bundle, 95/95	[ ]			] a.c.e	17.43
Whole Plant, 95/50	[ ]			] a.c.e	17.72
Whole Plant; 95/95	[ ]			] a.c.e	17.74

### 3.5 POISSON CONTRACTION EFFECT ON H\*

An evaluation was performed to determine the effect of end cap loading on H\* due to Poisson contraction of the tube. The pressure differential across the tube wall creates an effective end cap load, generating a positive axial stress state in the tube. This will cause a radial contraction of the tube via Poisson's ratio, which will necessarily reduce the contact pressure between the tube and tubesheet, hence increasing H\*. The purpose of this section of the report is to address the impact of Poisson contraction on the values calculated for H\* using the C<sup>2</sup> model.

#### 3.5.1 Methods Discussion

The method used to evaluate the effect of Poisson's ratio on H\* is a simplified approach using approximations to determine the reduction in contact pressure. A classical thick-shell formula is used to calculate the change in radius due to Poisson's ratio effects from an applied end cap load. This change in radius is directly converted to a contact pressure utilizing the thick shell equations in References 3-1 and 3-2. This contact pressure is then subtracted from the contact pressure curve calculated in Reference 3-8. The difference is reported and discussed. All calculations for Poisson's contraction are based on an end cap load without a factor of safety, as it is unrealistic to apply a factor of safety to a physical effect such as Poisson's contraction. The end cap load used to generate H\*, however, continues to include the appropriate factor (3.0 for 100 percent power, 1.4 for SLB).

#### 3.5.2 Discussion of Significant Assumptions

The limiting plant for each model SG, as defined in References 3-1 and 3-2 is assumed to have the limiting Poisson effect. This is reasonable because, in part, the limiting plant is determined by that with the highest end cap load.

One hundred percent power and NOP were determined to be the limiting conditions in References 3-1 and 3-2 for H\* for the Model 44F and the Model 51F SGs. Consistent with those analyses, these conditions were examined.

#### 3.5.3 Input

The input for this analysis consists of steam generator dimensions for the plants to be analyzed, material properties from the ASME code, and pressure and temperature conditions from the PCWG parameters.

The end cap loads for the different model SGs, Table 3-32, are taken from References 3-1 and 3-2. The modulus of elasticity is the same as in the FEA, in Table 3-3. Poisson's ratio for Alloy 600 is [ ]<sup>a,c,e</sup> as taken from the ASME code, Reference 3-12.

Material properties were taken at temperatures consistent with those used in the FEA discussed in Section 3.1. Material properties are taken at [ ]<sup>a,c,e</sup> °F for 100 percent power for all plants.

### 3.5.4 Calculation of Radial Dilation

From Reference 3-16 (Page 396), the radial dilation of a pressurized thick-wall cylinder is given by:

$$\Delta R = \frac{r}{E_t(r_o^2 - r_i^2)} \left[ (1 - 2\nu)(p_i r_i^2 - p_o r_o^2) + (1 + \nu) \frac{r_i^2 r_o^2 (p_i - p_o)}{r^2} - \frac{\nu P}{\pi} \right] \quad (\text{Equation 3-10})$$

Where

P = Endcap load (pounds)

$\nu$  = Poisson's ratio

r = Radial coordinate (inches)

$r_o$  = Outer radius of tube (inches)

$r_i$  = Inner radius of tube (inches)

$p_i$  = Pressure on inside of tube (psi)

$p_o$  = Pressure on outside of tube (psi)

$E_t$  = Elastic Modulus of tube (psi)

$\pi$  = pi (3.14159)

$\Delta R$  = change in radial coordinate due to loadings (inches)

P is the end cap load, in pounds.

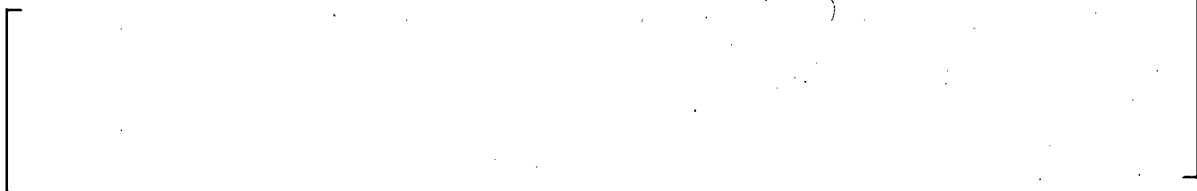
Since the figure of interest is the radial contact at the outside radius due to the applied end cap load, the difference is:

$$\Delta R_{endcap} = -\frac{r_o \nu P}{E \pi (r_o^2 - r_i^2)} \quad (\text{Equation 3-11})$$

This equation is used to calculate radial dilations due to the Poisson contraction alone (Table 3-32). As can be seen, there is a small radial contraction (approximately [ ]<sup>a,c,e</sup> micro-inches) due to Poisson effects.

### 3.5.5 Calculation of Contact Pressure Reduction from Poisson Effect

The contact pressure change due to Poisson effects can be estimated by using the thick shell equations from References 3-1 and 3-2. The thick shell formula is (page 6-91 of Reference 3-1):



(Equation 3-12)

Where

- $P_i$  =Internal primary side pressure, psi  
 $P_{crev}$  =Crevice pressure, psi  
 $r_i$  =Inside radius of tube, in  
 $r_o$  =Outside radius of tube, in  
 $\alpha_t$  =Coefficient of thermal expansion of tube, in/in/°F  
 $E_t$  =Modulus of Elasticity of tube, psi  
 $E_{ts}$  =Modulus of Elasticity of tubesheet, psi  
 $T_t$  =Temperature of tube, °F, and,  
 $\nu$  =Poisson's Ratio of the material.  
 $P_{contact}$  =Contact Pressure  
 $D$  =Outside radius of cylinder which provides the same radial stiffness as the tubesheet

As can be seen, the thick shell equation for contact pressure is simply a sum of radial displacements divided by an effective elastic constant. This makes intuitive sense because the physical interpretation of the thick shell equations is as follows:

1. Apply internal pressure, crevice pressure, and thermal loads to a free tube which has a nominal outside diameter equivalent to the collar bore ID. Calculate the resultant radial dilation.
2. Calculate the bore displacement of a free collar from crevice pressure and the applied dilation from the 3-D FEA model.
3. If the answers to one and two above possess a geometric interference (the resultant tube radius is larger than the bore), then there exists positive contact pressure. The positive contact pressure can be calculated as that pressure which, when applied to both the tube OD and the collar ID, eliminates the geometric interference, producing line-on-line contact.

In step 3, it is clear that the relationship between contact pressure and radial geometric interference should be linear, as the thick shell equations are linear elastic. Therefore, it is appropriate to calculate contact

pressure reduction by simply dividing the differential radial displacement due to Poisson's ratio effects by the elastic constant in the denominator above:

$$\left[ \frac{\Delta r}{r} \right]^{a,c,e} \quad \text{(Equation 3-13)}$$

Results of the calculation of the elastic constants are provided in Table 3-33 for Model 51F and 3-loop Model 44F SG operating conditions. Substituting the differential radial dilation from Table 3-32 into the above equation yields the contact pressure reductions shown in Table 3-34. As can be seen, there are modest reductions of approximately [ ]<sup>a,c,e</sup> psi at 100 percent power and approximately twice that (~[ ]<sup>a,c,e</sup> psi) at SLB conditions. This makes intuitive sense because the Poisson' contraction is proportional to the stress, which is proportional to the pressure differential, and the SLB delta-p is approximately twice that of 100 percent power.

### 3.5.6 Calculation of Increase in H\* Values

In order to calculate the change in H\* values due to the decreased contact pressure, the contact pressure curves from Section 3.3 must be reduced by the above contact pressures and integrated again to find the change in H\*. In each case, only the critical radius was evaluated for each model. The reference square cell analysis (Section 3.3) explains the methodology for calculating H\*. The formula for pull out load is

$$F = \int \mu \pi d_o P_{contact} dy \quad \text{(Equation 3-14)}$$

Where  $\mu$  is the coefficient of friction, chosen to be [ ]<sup>a,c,e</sup> in the licensing basis analysis.

Calculations for the increased H\* for each model are in Table 3-35 and Table 3-36, and a sample chart is in Figure 3-41. In each case, the contact pressure curve is shifted down by the appropriate amount and H\* recalculated. Baseline numbers from Reference 3-9 are included for comparison. As can be seen, the increase in H\* due to Poisson effects amounts to approximately [ ]<sup>a,c,e</sup> inches (before attenuation). This value assumes Poisson contraction occurs along the entire length. A more realistic calculation will account for the Poisson effect attenuating after an accumulated pull out resistance equal to the end cap load is attained. This correction is obtained by interpolation using the same methodology as for H\*, but with an end cap load that does not have a factor of safety. The interpolated attenuation distances are in Table 3-44.

The next step in the process is to calculate new H\* values with contact pressures that are reduced only inside the attenuation distance. This involves interpolating the contact pressure and shifting only a portion of it. Calculations are tabulated in Tables 3-37 through 3-41. A summary of the Final H\* values after adjusting for Poisson contraction and attenuation are in Table 3-42. As can be seen, the greatest difference is approximately [ ]<sup>a,c,e</sup> inches.

However, this is for mean H\* values. The final figure of interest is the effect that Poisson contraction has on the probabilistic, or extreme H\* values. Calculations for the probabilistic values are in Tables 3-41

through Table 3-45. A summary of the effect of Poisson's contraction on H\* is in Table 3-46. As can be seen, the largest effect is [ ]<sup>a,c,e</sup> inch for the Model 44F SG ([ ]<sup>a,c,e</sup> inch for the Model 51F).

**Table 3-32 Calculation of Radial Dilation Due to Poisson Effects Model 51F and 3-Loop 44F SGs**

Parameter	Model 51F		Model 44F		
	100% Power		100% Power		
Tube R <sub>i</sub> (in)					a,c,e
Tube R <sub>o</sub> (in)					
E <sub>tube</sub> (Msi)					
Endcap Load (lbs)					
Delta-R (micro-inch)					

**Table 3-33 Calculation of Elastic Constants**

Parameter	Model 51F		Model 44F		
	100% Power	SLB	100% Power	SLB	
Tube r <sub>i</sub> (in)					a,c,e
Tube r <sub>o</sub> (in)					
Collar R <sub>o</sub> (in)					
Tube E (Msi)					
Tubesheet E (Msi)					
v					
Elastic Constant (in <sup>3</sup> /lb)					

**Table 3-34 Calculation of Reduction in Contact Pressure from Poisson Effects**

Parameter	Model 51F	Model 44F
	100% Power	100% Power
$\Delta r$ due to $\nu$ ( $\mu\text{in}$ )		
Elastic Constant ( $\text{in}^3/\text{lb}$ )		
$P_{\text{con}}$ Reduction (psi)		

a,c,e

**Table 3-35 Baseline and Adjusted  $H^*$  Calculation for Model 51F (Surry Units 1 & 2)**

100% Power, [ ] <sup>a,c,e</sup> in Radius				
End cap load = [ ] <sup>a,c,e</sup> pounds				
Elevation	Baseline		Shifted due to Poisson	
	$P_{\text{con}}$ (psi)	Accumulated Pull Out Load (pounds)	$P_{\text{con}}$ (psi)	Accumulated Pull Out Load (pounds)
0 <sup>(1)</sup>				
2				
4				
6				
10.515				
16.901				
19.03				
20.03				
21.03 <sup>(2)</sup>				
$H^*$ (inches)				

Notes: (1) Bottom of Tubesheet  
(2) Top of Tubesheet

a,c,e

**Table 3-36 Baseline and Adjusted H\* Calculation for Model 44F (Turkey Point Units 3 & 4)**

100% Power, [ ] <sup>a,c,e</sup> in Radius				
Endcap load = [ ] <sup>a,c,e</sup> pounds				
Elevation	Baseline		Shifted due to Poisson	
	P <sub>con</sub> (psi)	Accumulated Pull Out Load (pounds)	P <sub>con</sub> (psi)	Accumulated Pull Out Load (pounds)
0 <sup>(1)</sup>				
2				
3.523				
5.442				
10.905				
16.368				
18.287				
19.81				
21.81 <sup>(2)</sup>				
H* (inches)				

a,c,e

Notes: (1) Bottom of Tubesheet  
(2) Top of Tubesheet

**Table 3-37 Distance for Poisson Effect to Attenuate**

Model SG	51F	44F
Distance for Poisson Effect to Attenuate (inches)	[	] <sup>a,c,e</sup>

**Table 3-38 H\* Calculation for Model 51F Including Poisson Attenuation (Surry Units 1&2)**

Model 51F, 100% Power, [ ] <sup>a,c,e</sup> in Radius		
End cap load = [ ] <sup>a,c,e</sup> pounds		
Elevation	P <sub>con</sub> (psi)	Accumulated Pull Out Load (pounds) <sub>a,c,e</sub>
0 <sup>(1)</sup>		
2		
4		
6		
10.515		
14.467		
16.901		
19.03		
20.03		
21.03 <sup>(2)</sup>		
H* (inches)		
Notes: (1) Bottom of Tubesheet (2) Top of Tubesheet		

**Table 3-39 H\* Calculation for Model 44F including Poisson Attenuation (Turkey Point Units 3 & 4)**

Model 44F, 100% Power, [ ] <sup>a,c,e</sup> Radius		
End cap load = [ ] <sup>a,c,e</sup> pounds		
Elevation	P <sub>con</sub> (psi)	Accumulated Pull Out Load (pounds) <sub>a,c,e</sub>
0 <sup>(1)</sup>		
2		
3.523		
5.442		
10.905		
15.926		
16.368		
18.287		
19.81		
21.81 <sup>(2)</sup>		
H* (inches)		
Notes: (1) Bottom of Tubesheet (2) Top of Tubesheet		

**Table 3-40 Comparison of Mean H\* Values**

Parameter	Model 51F	Model 44F
H* Unmodified		
H* + Poisson		
H* + Poisson + Attenuation		
Final Difference		

**Table 3-41 Baseline and Adjusted H\* Calculation for Model 51F (Surry Units 1 & 2)**

(MC rank [ ]<sup>a,c,e</sup>) :

100% Power, [ ] <sup>a,c,e</sup> in Radius				
End cap load = [ ] <sup>a,c,e</sup> pounds				
Elevation	Baseline		Shifted due to Poisson	
	P <sub>con</sub> (psi)	Accumulated Pull Out Load (pounds)	P <sub>con</sub> (psi)	Accumulated Pull Out Load (pounds) <sub>a,c,e</sub>
0 <sup>(1)</sup>				
2				
4				
6				
10.515				
16.901				
19.03				
20.03				
21.03 <sup>(2)</sup>				
H* (inches)				

Notes: (1) Bottom of Tubesheet  
(2) Top of Tubesheet

**Table 3-42 Baseline and Adjusted H\* Calculation for Model 44F (Turkey Point Units 3 & 4)**

(MC Rank [ ]<sup>a,c,e</sup>)

100% Power, [ ] <sup>a,c,e</sup> in Radius						
End cap load = [ ] <sup>a,c,e</sup> pounds						
Elevation	Baseline			Shifted due to Poisson		
	P <sub>con</sub> (psi)	Accumulated Pull Out Load (pounds)		P <sub>con</sub> (psi)	Accumulated Pull Out Load (pounds) <sub>a,c,e</sub>	
0 <sup>(1)</sup>						
2						
3.523						
5.442						
10.905						
16.368						
18.287						
19.81						
-21.81 <sup>(2)</sup>						
H* (inches)						

Notes: (1) Bottom of Tubesheet  
(2) Top of Tubesheet

**Table 3-43 Distance for Poisson Effect to Attenuate Probabilistic H\* Values**

Model SG	51F	44F
Distance for Poisson Effect to Attenuate (inches)	[ ]	] <sup>a,c,e</sup>

**Table 3-44 H\* Calculation for Model 51F including Poisson Attenuation (Surry Units 1 & 2)**

(MC rank [ ]<sup>a,c,e</sup>)

100% Power, [ ] <sup>a,c,e</sup> in Radius		
End cap load = [ ] <sup>a,c,e</sup> pounds		
Elevation	P <sub>con</sub> (psi)	Accumulated Pull Out Load (pounds)
0 <sup>(1)</sup>		
2		
4		
6		
7.16		
10.515		
16.901		
19.03		
20.03		
21.03 <sup>(2)</sup>		
H* (inches)		
Notes: (1) Bottom of Tubesheet (2) Top of Tubesheet		

**Table 3-45 H\* Calculation for Model 44F Including Poisson Attenuation (Turkey Point Units 3 & 4)**

(MC rank [ ]<sup>a,c,e</sup>)

Model 44F, [ ] <sup>a,c,e</sup> in Radius		
Endcap load = [ ] <sup>a,c,e</sup> pounds		
Elevation	P <sub>con</sub> (psi)	Accumulated Pull Out Load (pounds)
0 <sup>(1)</sup>		
2		
3.523		
5.442		
9.48		
10.905		
16.368		
18.287		
19.81		
21.81 <sup>(2)</sup>		
H* (inches)		

Notes: (1) Bottom of Tubesheet  
(2) Top of Tubesheet

**Table 3-46 Comparison of Probabilistic H\* Values (inches)**

Parameter	Model 51F	Model 44F
H* Unmodified		
H* + Poisson		
H* + Poisson + Attenuation		
Final Difference		



**Figure 3-41 Effect of Poisson Contraction on Contact Pressure**

---

### 3.6 REFERENCES

- 3-1. WCAP-17091-P, Revision 0, "H\*: Alternate Repair Criteria for the Tubesheet Expansion Region in Steam Generators with Hydraulically Expanded Tubes (Model 44F)," June 2009.
- 3-2. WCAP-17092-P, Revision 0, "H\*: Alternate Repair Criteria for the Tubesheet Expansion Region in Steam Generators with Hydraulically Expanded Tubes (Model 51F)," June 2009.
- 3-3. WTD-SM-75-072, "Temperature Distributions for Calculation of Secondary Skin Stress in D2-D3 Tubesheet Analysis," August 1975.
- 3-4. Report 1014982, "Divider Plate Cracking in Steam Generators: Results of Phase I: Analysis of Primary Water Stress Corrosion Cracking and Mechanical Fatigue in the Alloy 600 Stub Runner to Divider Plate Weld Material," EPRI, Palo Alto, CA; 2007.
- 3-5. Jaluria, Yogesh, "Computer Methods for Engineering," Taylor and Francis, 1996.
- 3-6. CN-SGMP-10-15, Revision 1, "3-D Finite Element Analysis of Limiting Plants for H\* with Thermal Profile," November 2010.
- 3-7. WNET-150, Volume 3, "Model E2, Steam Generator Stress Report, Primary Chamber Components Interactions Analysis," December 1978
- 3-8. CN-SGMP-10-3 Revision 0, "Square Cell Finite Element Analyses for Models D5, F, 44F and 51F Plants for H\*," October 2010.
- 3-9. LTR-SGMP-09-104, Revision 1, "White Paper: H\* Values at More Restrictive Probabilistic Criteria," August 13, 2009.
- 3-10. A.C. Atkinson, *The Design of Experiments to Estimate the Slope of a Response Surface*, Biometrika 1970, Volume 57, Issue 2, pg. 319.
- 3-11. Not used.
- 3-12. ASME B&PV Code, 2007 edition, no addenda, Section II, Part D, Subpart 2: Physical Properties Tables, Table PRD.
- 3-13. LTR-SGMP-09-100 P-Attachment, Revision 1, "Response to NRC Request for Additional Information on H\*; Model F and Model D5 Steam Generators," September 7, 2010.
- 3-14. *Statistics, Probability and Reliability for Civil and Environmental Engineers*, Kottogoda, N.T., Rosso, R., McGraw-Hill, © 1997.
- 3-15. Westinghouse Drawing 1105J05, Revision 3, "Tube Plate Drilling."

---

3-16. *Advanced Mechanics of Materials*, Boresi, Arthur P and Schmidt, Richard J, Sixth Edition, John Wiley and Sons Publishing

## 4 C<sup>2</sup> MODEL LEAKAGE INTEGRITY DISCUSSION

As noted in References 4-1 and 4-2, the licensing basis for the plants with Model 44F and Model 51F steam generators does not include considerations of the feedwater line break (FLB) transient; therefore it necessary to consider only the SLB transient in the development of the accident induced to normal operating leakage factors.

The model for leakage applied in References 4-1, 4-2, and 4-3 is the Darcy formulation for flow through a porous medium. The Darcy equation is:

$$Q = \frac{\Delta p}{12\mu Kl} \quad (\text{Equation 4-1})$$

Where

$\Delta p$  is the driving potential (primary-to-secondary pressure difference)

$\mu$  is the fluid dynamic viscosity

$K$  is the loss coefficient for flow through the porous medium

$l$  is the length of the porous medium

The Darcy formulation (Equation 4-1) is used in References 4-1, 4-2, and 4-3 to develop the ratio of leak rates between postulated accident induced conditions and normal operating conditions (NOP). The resulting Darcy flow equation ratio can be separated into four "subfactors" as follows:

$$\frac{Q_{DBA}}{Q_{NOP}} = \frac{\Delta p_{DBA}}{\Delta p_{NOP}} \frac{\mu_{NOP}}{\mu_{DBA}} \frac{K_{NOP}}{K_{DBA}} \frac{l_{NOP}}{l_{DBA}} \quad (\text{Equation 4-2})$$

The purpose of this section of the report is to address the impact of the new square cell model results on the existing licensing basis leak rate factors provided in Reference 4-3 for the Model 44F and Model 51F steam generators in 3-loop plants. It was determined that application of the square cell model results does not affect any of the four subfactors identified in Equation 4-2 above; therefore, the leakage factors established in the current licensing basis are unchanged.

The driving head ( $\Delta p$ ) at both NOP and SLB conditions are known and remain unchanged from the current licensing basis. Also, the temperatures and pressures, which define the fluid viscosity ( $\mu$ ), remain the same. Therefore, the pressure and viscosity subfactors in Equation 4-2 above remain unchanged.

As discussed in Section 9.1.1 of References 4-1 and 4-2, the current licensing basis leakage factors assume a loss coefficient subfactor of 1.0. The available data for hydraulically expanded tubes in tubesheet simulants (References 4-4 and 4-5), both at room temperature and at elevated temperature, are utilized in References 4-1 through 4-3 to show that no correlation between loss coefficient and contact pressure exists for conditions that simulate the Model D5 SG conditions. However, because the data exhibit considerable scatter, confidence in this data analysis is low. Engineering judgment could suggest that loss coefficient might be related to the absolute contact pressure between the tubes and the tubesheet. Hence, a requirement was applied to the H\* leakage analysis by the regulatory authorities that it is necessary to show that the contact pressure at accident induced conditions exceeds the contact pressure at normal operating conditions ( $P_{C_{FLB/SLB}}:P_{C_{NOP}} > 1$ ) in order to assume that the loss coefficient subfactor is equal to 1.0.

For both the Model 44F and 51F steam generators in 3 loop plants, the results of the square cell analysis show that the contact pressure during steam line break conditions at various elevations between 0 and 21.81 (Model 44F)/21.03 (Model 51F) inches at all radii in the tube bundle always meets or exceeds the contact pressure above the H\* distance from the top of the tubesheet during normal operating conditions as shown on Figures 3-18 through 3-23 for the Model 44F steam generator and Figures 3-24 through 3-29 for the Model 51F steam generator, thereby meeting the intent of the criterion ( $P_{C_{SLB}}:P_{C_{NOP}} > 1$ ). Therefore, it is concluded that it is acceptable to apply a loss coefficient subfactor,  $K_{NOP}/K_{DBA}$  of 1.0.

Addressing the effective crevice length subfactor, as discussed in References 4-1 and 4-2, recall that "effective crevice length" is defined as the length of positive contact between the tube and the tubesheet (above H\*). Again, based on a review of Figures 3-18 to 3-23 for the Model 44F steam generator and Figures 3-24 through 3-29 for the Model 51F steam generator, the effective crevice length during a postulated SLB event meets or exceeds the effective length of crevice for normal operating conditions for the Model 44F/51F steam generators in 3-loop plants. Therefore, the effective length ratio subfactor for ( $l_{NOP}/l_{DBA}$ ) can be assumed to be 1.0 during a postulated steam line break event for the Model 44F and Model 51F steam generators.

As discussed in References 4-1 and 4-2, the design specification curves for the locked rotor and control rod ejection events apply for the leakage factors for these transients. These transients are of very short duration, for which the H\* leakage calculations employ a time integrated leakage approach. The same leakage factors (< 1.0) for a postulated locked rotor and control rod ejection event for the Model 44F and 51F SGs in the H\* fleet included in Reference 4-3 continue to apply.

Based on the above, it is concluded that the current licensing basis leakage factors identified in Reference 4-3 continue to apply when considering the C<sup>2</sup> model results.

---

## 4.1 REFERENCES

- 4-1 WCAP-17091-P, Revision 0 "H\*: Alternate Repair Criteria for the Tubesheet Expansion Region in Steam Generators with Hydraulically Expanded Tubes (Model 44F)," June 2009.
- 4-2 WCAP-17092-P, Revision 0 "H\*: Alternate Repair Criteria for the Tubesheet Expansion Region in Steam Generators with Hydraulically Expanded Tubes (Model 51F)," June 2009.
- 4-3 LTR-SGMP-09-100 P-Attachment, Revision 1 "Response to NRC Request for Additional Information on H\*; Model F and Model D5 Steam Generators," September 7, 2010.
- 4-4 CN-SGDA-03-119, "Calculation of Loss Coefficient for Model D5 Steam Generators," Westinghouse Electric Company LLC, November 10 2003.
- 4-5 STD-MCE-03-49, "Determination of the Model D5 Tube-to-Tubesheet Leakage Resistance for H-star Program for CBE/CDE/DDP/TCX," November 4, 2003.

---

## 5 REPORT SUMMARY AND CONCLUSIONS

The purpose of this report is to provide final resolution of the NRC technical issue regarding tubesheet bore eccentricity on the H\* criterion. As a result, the NRC staff asked 14 questions related to this issue. As stated in Section 1.0 of this report, the content of this report primarily focuses on resolving NRC Request for Additional Information (RAI) #5 and #12. A roadmap was provided in Section 1.0 to previous documents issued by Westinghouse in response to the remainder of the 14 RAI.

There are two principal requirements for H\*:

1. Assure that tube(s) do not pull out of the tubesheet under the most limiting loadings during normal or accident conditions.
2. Assure that primary-to-secondary coolant leakage through the tube-to-tubesheet crevice is no greater than that assumed in the final safety analysis report (FSAR) for the most limiting accident.

Concerning item 1, the Westinghouse action plan to resolve the NRC staff tube pull out concerns relating to tube bore eccentricity involved the development of a more accurate analysis model for calculating tube joint contact pressure. As discussed in Section 3.0 of this report, the square cell ( $C^2$ ) model analysis is an independent method of modeling the contact pressure distribution between the tube and the tubesheet throughout the tubesheet thickness.

For the Model 44F SG in 3 loop plants, the value of H\* inspection depth required to meet the structural integrity goals of the plant increased by 2.71 inches. The value for the H\* inspection depth for the Model 51F SGs increased by 2.16 inches. The differences between the two models are the results of different tubesheet thicknesses, tubesheet displacements and contact pressure distributions. A direct comparison between the licensing basis probabilistic H\* values and the square cell analysis probabilistic H\* values for the Model 44F and Model 51F steam generators is shown in Table 5-1. The H\* values in Table 5-1 provide tube pull out capability that meet or exceed the structural integrity acceptance criteria identified in Section 4.1 of References 5-1 and 5-2.

The impact of the new square cell model results on the existing licensing basis leak rate factors provided in Reference 5-3 for the Model 44F and Model 51F steam generators in 3-loop plants was evaluated. It has been determined that the square cell model results do not affect the current licensing basis leakage rate factors. The driving heads ( $\Delta p$ ) at NOP and SLB conditions are known and remain unchanged from the current licensing basis as well as the temperatures and pressures remain the same to define the fluid viscosity ( $\mu$ ). Therefore, the pressure and viscosity subfactors remain unchanged.

The results of the square cell analysis show that the contact pressure during steam line break conditions at various elevations between 0 and 21.81 (Model 44F)/21.03 (Model 51F) inches at all radii in the tube bundle always meets or exceeds the contact pressure above the H\* distance from the top of the tubesheet during normal operating conditions. Therefore, it is concluded that it is acceptable to apply a loss coefficient subfactor,  $K_{NOP}/K_{DBA}$  of 1.0. Also, the effective crevice length during a postulated SLB event meets or exceeds the effective length of crevice for normal operating conditions for the Model 44F/51F steam generators in 3-loop plants. Therefore, the effective length ratio subfactor for ( $l_{NOP}/l_{DBA}$ ) can be assumed to be 1.0 during a postulated steam line break event for the Model 44F/51F steam generators.

---

Concerning all other design basis accidents that model accident condition leakage, as discussed in References 5-1 and 5-2, the design specification curves for the locked rotor and control rod ejection events apply for the leakage factors for these transients. These transients are of very short duration and the H\* leakage calculations employ a time integrated leakage approach. The same leakage factors for a postulated locked rotor and control rod ejection event for the Model 44F and 51F SGs included in the current licensing basis (Reference 5-3) continue to apply.

Based on the above, with the use the leakage factors included in the current licensing basis (Reference 5-3), it is concluded that primary-to-secondary leakage through the tube-to-tubesheet crevice is bounded by the values assumed in the final safety analysis report (FSAR) for the most limiting accident.

Satisfactory resolution of the NRC technical issue regarding tubesheet bore eccentricity is complete. Together with documents provided under separate cover, (e.g., Reference 5-4) this document completes the response to the RAI provided in Reference 5-5. Application of the C<sup>2</sup> model has provided independent confirmation that the structural criteria are met. Probabilistic H\* values were re-calculated based on application of the C<sup>2</sup> model and substantially confirm the values contained in the current licensing basis. The differences between the H\* results based on the C<sup>2</sup> model and those from the prior application of the thick shell model are explained. The leakage factors contained in the current licensing basis for the Model 44F and Model 51F SGs are shown to be conservative and acceptable for implementation of H\*.

**Table 5-1 Results of Probabilistic Comparison Study for the Limiting Plants for Models 44F and 51F**

SG Model/ Limiting Plant	Limiting Operating Condition	Current Licensing Basis	Thick Shell Calculations			Square Cell Calculations			
			(Reference 5-6)		Implemented H* (1)	Whole Bundle		Whole Plant	
			95/50 Whole Bundle	95/95 Whole Plant		95/50	95/95	95/50	95/95
			in	in	in	in	in	in	in
Model 44F / Turkey Point 3&4	NOP	WCAP - 17091-P	13.31	15.09	17.28			a,c,e 17.79	17.80
Model 51F/ Surry 1& 2	NOP	WCAP- 17092-P	13.14	15.58	16.7			17.72	17.74
Notes:									
(1) Values taken from utilities' 2009 license amendment requests.									

---

## 5.1 REFERENCES

- 5-1. WCAP-17091-P, Revision 0, "H\*: Alternate Repair Criteria for the Tubesheet Expansion Region in Steam Generators with Hydraulically expanded Tubes (Model 44F)", June 2009.
- 5-2. WCAP-17092-P, Revision 0, "H\*: Alternate Repair Criteria for the Tubesheet Expansion Region in Steam Generators with Hydraulically expanded Tubes (Model 51F)," June 2009.
- 5-3. LTR-SGMP-09-100 P-Attachment, Revision 1, "Response to NRC Request for Additional Information H\*; Model F and Model D5 Steam Generators," September 7, 2009.
- 5-4. LTR-SGMP-10-33 P-Attachment, "H\*: Response to NRC Questions Regarding Tubesheet Bore Eccentricity," September 2010.
- 5-5. USNRC Letter, "Vogtle Electric Generating Plant, Units 1 and 2 – Transmittal of Unresolved Issues Regarding Permanent Alternate Repair Criteria for Steam Generators (TAC Nos. ME 1339 and ME 1340)," November 23, 2009.
- 5-6. LTR-SGMP-09-104 P-Attachment, Revision 1, "White Paper on Probabilistic Assessment of H\*," August 13, 2009.

**Attachment 6**

**Westinghouse Electric Company LLC LTR-CAW-10-3014,  
"Application for Withholding Proprietary Information from  
Public Disclosure," dated November 15, 2010**

**Virginia Electric and Power Company  
(Dominion)  
Surry Power Station Unit 2**



Westinghouse Electric Company  
Nuclear Services  
1000 Westinghouse Drive  
Cranberry Township, PA 16066  
USA

U.S. Nuclear Regulatory Commission  
Document Control Desk  
Washington, DC 20555-0001

Direct tel: (412) 374-4643  
Direct fax: (724) 720-0754  
e-mail: greshaja@westinghouse.com  
Proj letter: VRA-10-63

CAW-10-3014

November 15, 2010

APPLICATION FOR WITHHOLDING PROPRIETARY  
INFORMATION FROM PUBLIC DISCLOSURE

Subject: WCAP-17345-P, "H\*: Resolution of NRC Technical Issue Regarding Tubesheet Bore Eccentricity (Model 44F 3-Loop and Model 51F)" (Proprietary)

The proprietary information for which withholding is being requested in the above-referenced report is further identified in Affidavit CAW-10-3014 signed by the owner of the proprietary information, Westinghouse Electric Company LLC. The affidavit, which accompanies this letter, sets forth the basis on which the information may be withheld from public disclosure by the Commission and addresses with specificity the considerations listed in paragraph (b)(4) of 10 CFR Section 2.390 of the Commission's regulations.

Accordingly, this letter authorizes the utilization of the accompanying affidavit by Virginia Electric and Power Company.

Correspondence with respect to the proprietary aspects of the application for withholding or the Westinghouse affidavit should reference this letter, CAW-10-3014, and should be addressed to J. A. Gresham, Manager, Regulatory Compliance and Plant Licensing, Westinghouse Electric Company LLC, Suite 428, 1000 Westinghouse Drive, Cranberry Township, PA 16066.

Very truly yours,

A handwritten signature in black ink, appearing to read 'J. A. Gresham'.

J. A. Gresham, Manager  
Regulatory Compliance and Plant Licensing

Enclosures

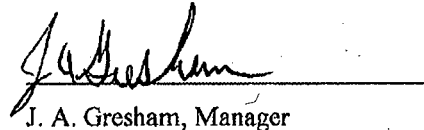
AFFIDAVIT

COMMONWEALTH OF PENNSYLVANIA:

ss

COUNTY OF BUTLER:

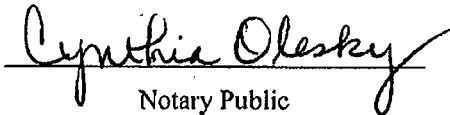
Before me, the undersigned authority, personally appeared J. A. Gresham, who, being by me duly sworn according to law, deposes and says that he is authorized to execute this Affidavit on behalf of Westinghouse Electric Company LLC (Westinghouse), and that the averments of fact set forth in this Affidavit are true and correct to the best of his knowledge, information, and belief:



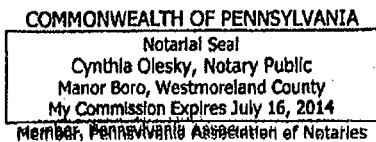
J. A. Gresham, Manager

Regulatory Compliance and Plant Licensing

Sworn to and subscribed before me  
this 15th day of November 2010



Notary Public



- (1) I am Manager, Regulatory Compliance and Plant Licensing, in Nuclear Services, Westinghouse Electric Company LLC (Westinghouse), and as such, I have been specifically delegated the function of reviewing the proprietary information sought to be withheld from public disclosure in connection with nuclear power plant licensing and rule making proceedings, and am authorized to apply for its withholding on behalf of Westinghouse.
- (2) I am making this Affidavit in conformance with the provisions of 10 CFR Section 2.390 of the Commission's regulations and in conjunction with the Westinghouse Application for Withholding Proprietary Information from Public Disclosure accompanying this Affidavit.
- (3) I have personal knowledge of the criteria and procedures utilized by Westinghouse in designating information as a trade secret, privileged or as confidential commercial or financial information.
- (4) Pursuant to the provisions of paragraph (b)(4) of Section 2.390 of the Commission's regulations, the following is furnished for consideration by the Commission in determining whether the information sought to be withheld from public disclosure should be withheld.
  - (i) The information sought to be withheld from public disclosure is owned and has been held in confidence by Westinghouse.
  - (ii) The information is of a type customarily held in confidence by Westinghouse and not customarily disclosed to the public. Westinghouse has a rational basis for determining the types of information customarily held in confidence by it and, in that connection, utilizes a system to determine when and whether to hold certain types of information in confidence. The application of that system and the substance of that system constitutes Westinghouse policy and provides the rational basis required.

Under that system, information is held in confidence if it falls in one or more of several types, the release of which might result in the loss of an existing or potential competitive advantage, as follows:

    - (a) The information reveals the distinguishing aspects of a process (or component, structure, tool, method, etc.) where prevention of its use by any of

Westinghouse's competitors without license from Westinghouse constitutes a competitive economic advantage over other companies.

- (b) It consists of supporting data, including test data, relative to a process (or component, structure, tool, method, etc.), the application of which data secures a competitive economic advantage, e.g., by optimization or improved marketability.
- (c) Its use by a competitor would reduce his expenditure of resources or improve his competitive position in the design, manufacture, shipment, installation, assurance of quality, or licensing a similar product.
- (d) It reveals cost or price information, production capacities, budget levels, or commercial strategies of Westinghouse, its customers or suppliers.
- (e) It reveals aspects of past, present, or future Westinghouse or customer funded development plans and programs of potential commercial value to Westinghouse.
- (f) It contains patentable ideas, for which patent protection may be desirable.

There are sound policy reasons behind the Westinghouse system which include the following:

- (a) The use of such information by Westinghouse gives Westinghouse a competitive advantage over its competitors. It is, therefore, withheld from disclosure to protect the Westinghouse competitive position.
- (b) It is information that is marketable in many ways. The extent to which such information is available to competitors diminishes the Westinghouse ability to sell products and services involving the use of the information.
- (c) Use by our competitor would put Westinghouse at a competitive disadvantage by reducing his expenditure of resources at our expense.

- (d) Each component of proprietary information pertinent to a particular competitive advantage is potentially as valuable as the total competitive advantage. If competitors acquire components of proprietary information, any one component may be the key to the entire puzzle, thereby depriving Westinghouse of a competitive advantage.
  - (e) Unrestricted disclosure would jeopardize the position of prominence of Westinghouse in the world market, and thereby give a market advantage to the competition of those countries.
  - (f) The Westinghouse capacity to invest corporate assets in research and development depends upon the success in obtaining and maintaining a competitive advantage.
- (iii) The information is being transmitted to the Commission in confidence and, under the provisions of 10 CFR Section 2.390; it is to be received in confidence by the Commission.
- (iv) The information sought to be protected is not available in public sources or available information has not been previously employed in the same original manner or method to the best of our knowledge and belief.
- (v) The proprietary information sought to be withheld in this submittal is that which is appropriately marked in WCAP-17345-P, "H\*: Resolution of NRC Technical Issue Regarding Tubesheet Bore Eccentricity (Model 44F 3-Loop and Model 51F)" (Proprietary), dated November 2010, for submittal to the Commission, being transmitted by Virginia Electric and Power Company Letter and Application for Withholding Proprietary Information from Public Disclosure, to the Document Control Desk. The proprietary information as submitted by Westinghouse for Surry Power Station, Units 1 and 2, is that associated with the technical justification of the H\* Alternate Repair Criteria for hydraulically expanded steam generator tubes and may be used only for that purpose.

This information is part of that which will enable Westinghouse to:

- (a) License the H\* Alternate Repair Criteria.

Further this information has substantial commercial value as follows:

- (a) Westinghouse plans to sell the use of the information to its customers for the purpose of licensing the H\* Alternate Repair Criteria.
- (b) Westinghouse can sell support and defense of the H\* criteria.
- (c) The information requested to be withheld reveals the distinguishing aspects of a methodology which was developed by Westinghouse.

Public disclosure of this proprietary information is likely to cause substantial harm to the competitive position of Westinghouse because it would enhance the ability of competitors to provide similar technical justification and licensing defense services for commercial power reactors without commensurate expenses. Also, public disclosure of the information would enable others to use the information to meet NRC requirements for licensing documentation without purchasing the right to use the information.

The development of the technology described in part by the information is the result of applying the results of many years of experience in an intensive Westinghouse effort and the expenditure of a considerable sum of money.

In order for competitors of Westinghouse to duplicate this information, similar technical programs would have to be performed and a significant manpower effort, having the requisite talent and experience, would have to be expended.

Further the deponent sayeth not.

### **PROPRIETARY INFORMATION NOTICE**

Transmitted herewith are proprietary and/or non-proprietary versions of documents furnished to the NRC in connection with requests for generic and/or plant-specific review and approval.

In order to conform to the requirements of 10 CFR 2.390 of the Commission's regulations concerning the protection of proprietary information so submitted to the NRC, the information which is proprietary in the proprietary versions is contained within brackets, and where the proprietary information has been deleted in the non-proprietary versions, only the brackets remain (the information that was contained within the brackets in the proprietary versions having been deleted). The justification for claiming the information so designated as proprietary is indicated in both versions by means of lower case letters (a) through (f) located as a superscript immediately following the brackets enclosing each item of information being identified as proprietary or in the margin opposite such information. These lower case letters refer to the types of information Westinghouse customarily holds in confidence identified in Sections (4)(ii)(a) through (4)(ii)(f) of the affidavit accompanying this transmittal pursuant to 10 CFR 2.390(b)(1).

### **COPYRIGHT NOTICE**

The reports transmitted herewith each bear a Westinghouse copyright notice. The NRC is permitted to make the number of copies of the information contained in these reports which are necessary for its internal use in connection with generic and plant-specific reviews and approvals as well as the issuance, denial, amendment, transfer, renewal, modification, suspension, revocation, or violation of a license, permit, order, or regulation subject to the requirements of 10 CFR 2.390 regarding restrictions on public disclosure to the extent such information has been identified as proprietary by Westinghouse, copyright protection notwithstanding. With respect to the non-proprietary versions of these reports, the NRC is permitted to make the number of copies beyond those necessary for its internal use which are necessary in order to have one copy available for public viewing in the appropriate docket files in the public document room in Washington, DC and in local public document rooms as may be required by NRC regulations if the number of copies submitted is insufficient for this purpose. Copies made by the NRC must include the copyright notice in all instances and the proprietary notice if the original was identified as proprietary.